Clumped isotope constraints on equilibrium carbonate formation and kinetic isotope effects in freezing soils

Landon K. Burgener [a,*], Katharine W. Huntington [a,*], Ronald Sletten [a], James M. Watkins [b], Jay Quade [c], Bernard Hallet [a]

[a] *Department of Earth and Space Sciences and Quaternary Research Center, University of Washington, Seattle, WA, USA*
[b] *Department of Earth Sciences, University of Oregon, Eugene, OR, USA*
[c] *Department of Geosciences, The University of Arizona, Tucson, AZ, USA*

Abstract

The clumped and stable isotope (Δ_{47}, $\delta^{18}O$, and $\delta^{13}C$) composition of pedogenic (soil) carbonates from cold, arid environments may be a valuable paleoclimate archive for climate change-sensitive areas at high latitudes or elevations. However, previous work suggests that the isotopic composition of cold-climate soil carbonates is susceptible to kinetic isotope effects (KIE). To evaluate the conditions under which KIE occur in cold-climate soil carbonates, we examine the Δ_{47}, $\delta^{18}O$, and $\delta^{13}C$ composition of soil carbonate pendants from Antarctica (Dry Valleys, 77°S), the High Arctic (Svalbard 79°N), the Chilean and Argentinian Andes, and the Tibetan plateau (3800–4800 m), and compare the results to local climate and water $\delta^{18}O$ records. At each site we calculate the expected equilibrium soil carbonate Δ_{47} and $\delta^{18}O$ values and estimate carbonate Δ_{47} and $\delta^{18}O$ anomalies (observed Δ_{47} or $\delta^{18}O$ minus the expected equilibrium Δ_{47} or $\delta^{18}O$). Additionally, we compare the measured carbonate $\delta^{13}C$ to the expected range of equilibrium soil carbonate $\delta^{13}C$ values. To provide context for interpreting the Δ_{47} and $\delta^{18}O$ anomalies, the soil carbonate results are compared to results for sub-glacial carbonates from two different sites, which exhibit large Δ_{47} anomalies (up to $-0.29‰$). The Antarctic and 4700 masl Chilean Andes samples have negative Δ_{47} anomalies and positive $\delta^{18}O$ anomalies consistent with KIE due to rapid bicarbonate dehydration during cryogenic carbonate formation. In contrast, the lower elevation Chilean Andes, Argentinian Andes, Tibetan Plateau and High Arctic results are consistent with equilibrium, summer carbonate formation. We attribute the differences in Δ_{47} and $\delta^{18}O$ anomalies to variations in inter-cobble matrix grain size and its effects on the effective soil pore space, permeability (hydraulic conductivity), moisture, and bicarbonate dehydration rate. The Antarctic and 4700 masl Chilean Andean soils have coarse-grained matrices that facilitate rapid bicarbonate dehydration. In contrast, the lower elevation Chilean Andes, Argentinian Andes, High Arctic and Tibetan Plateau soils have finer-grained matrices that decrease the soil pore space, soil permeability and CO_2 gas flux, promoting equilibrium carbonate formation. The sub-glacial carbonate samples yield highly variable Δ_{47} and $\delta^{18}O$ anomalies, and we propose that the differences between the two glacier sites may be due to variations in local sub-glacial drainage conditions, pCO_2, and pH. Our findings suggest that carbonates from soils with coarse-grained matrices may exhibit KIE in cold climates, making them poor paleoclimate proxies. Soils with fine-grained matrices are more likely to yield equilibrium carbonates suitable for paleoclimate reconstructions regardless of climate. Paleosol matrix grain size should therefore be taken into account in the evaluation of carbonate stable and clumped isotope values in paleoclimate studies.
© 2018 Elsevier Ltd. All rights reserved.

---

* Corresponding authors.
  E-mail addresses: lkb57@uw.edu (L.K. Burgener), kate1@uw.edu (K.W. Huntington).

1. INTRODUCTION

Pedogenic (formed in soil) carbonates are spatially and temporally abundant in the geologic record, and their isotopic compositions provide a rich archive of past climatic, environmental, and tectonic changes. Numerous studies have used carbonate stable ($\delta^{18}O$, $\delta^{13}C$) and clumped (Δ_{47}) isotope compositions to reconstruct the formation temperature, soil respiration and biologic productivity of modern soils and paleosols from a variety of geologic time periods to answer outstanding questions regarding paleoclimatology (e.g., Passey et al., 2010; Snell et al., 2013) and paleoaltimetry (e.g., Ghosh et al., 2006; Garzione et al., 2014; Carrapa et al., 2014; Licht et al., 2017). Most past studies of modern and ancient soil carbonates have typically focused on samples collected from temperate or warm environments (e.g., Gile et al., 1966; Gunal and Ransom, 2006; Quade et al., 2007; Hough et al., 2014; Diaz et al., 2016; Gallagher and Sheldon, 2016; Ringham et al., 2016; Dietrich et al., 2017). In contrast, a much smaller number of recent studies have investigated the clumped and stable isotope compositions of pedogenic carbonates from cold-climate soils (here defined as soils that experience sub-zero mean monthly temperatures for two or more consecutive months per year; e.g., Quade et al., 2011, 2013; Peters et al., 2013; Burgener et al., 2016). These cold-climate soil carbonates remain a largely untapped archive of climate information at high latitude and high elevation sites. Studies of cold-climate soil carbonates have the potential to expand the range of terrestrial environments that can be incorporated into paleotemperature reconstructions for a variety of applications. In particular, a better understanding of the processes by which soil carbonates form in cold climates is needed to confidently reconstruct environmental conditions from such samples, and ultimately to provide insight into topics such as the uplift history of continental plateaus or how polar amplification has affected high latitude areas during previous episodes of climate change.

Carbonate-based temperature reconstructions operate on principles of thermodynamic equilibrium. Soil carbonates forming in warm and/or temperate soils are generally regarded as forming under conditions approaching isotopic equilibrium due to the slow precipitation of soil carbonates (Breecker et al., 2009). In contrast, it has been proposed that the stable isotope and Δ_{47} records of some soil carbonates in cold climates may be complicated by isotopic disequilibrium due to kinetic isotope effects (KIE) (e.g., Courty et al., 1994; Burgener et al., 2016). Such KIE have been invoked to explain temperature-independent effects in cryogenic cave carbonates (e.g., Kluge et al., 2014), and in other types of cryogenic carbonates (e.g., Lacelle, 2007), and have been suggested by Burgener et al. (2016) to account for anomalously warm clumped isotope temperatures from the Tibetan Plateau (Quade et al., 2011). It is not known, however, whether such processes are widespread among soil carbonates forming in cold climates, or among sub-glacially precipitated carbonates.

The main objective of this study is to explore the mechanisms for soil carbonate formation in cold-climate soils, and to evaluate the extent to which disequilibrium occurs in such soil carbonates. To this end, we document variations in Δ_{47}, $\delta^{18}O$, and $\delta^{13}C$ values in a suite of soil carbonate pendants collected from diverse cold-climate environments, and compare these values to available modern soil and meteorological data. These comparisons enable us to (1) assess whether the soil carbonates are precipitating via "normal" processes typical of temperate soils (e.g., precipitation due to soil drying and subsequent $CaCO_3$ supersaturation of the soil solution), or via cryogenic processes (e.g., rapid soil water freezing leading to $CaCO_3$ supersaturation of the soil solution), and (2) evaluate how differences in environmental and soil conditions at the studied sites affect the magnitude of any observed KIE. The soil carbonates discussed in this study are pendant forms that precipitated on the underside of clasts collected from high-latitude sites in the Arctic and Antarctic, and from high-elevation sites in the Chilean and Argentinian Andes Mountains and the Tibetan Plateau (Fig. 1). To provide context for evaluating the magnitude of potential KIE for these
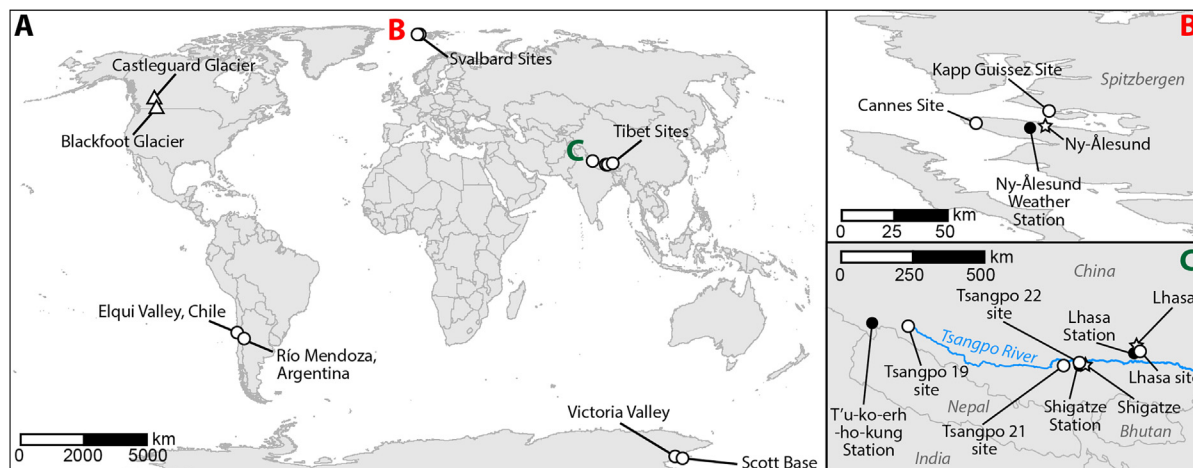

Fig. 1. (A) Index map showing the location of the soil sample sites (circles) and sub-glacial carbonate sample sites (triangles). (B) Spatial relationship between the two Svalbard soil sample sites (Cannes and Kapp Guissez) and the Ny-Ålesund weather station used to calculate local climate conditions. (C) Spatial relationship between the various Tibet soil sample sites and weather stations used to calculate local climate conditions (see Table 3).

samples, we compare the soil carbonate Δ_{47}, $\delta^{18}O$, and $\delta^{13}C$ values to the isotopic composition of cryogenic sub-glacial carbonates, which have well-constrained formation temperatures (between 0 and $-1\,°C$) and host water $\delta^{18}O$ values.

Our findings suggest that cold-climate soil carbonates are more likely to form under conditions of isotopic disequilibrium in soils with relatively coarse (e.g., sand to gravel) inter-cobble matrices, whereas isotopic equilibrium can be established in carbonates formed in soils with fine-grained (e.g., silt to sand) inter-cobble matrices. By constraining the degree to which cold-climate soil carbonates can be affected by disequilibrium processes, this study adds to a growing body of work which suggests that both soil moisture and soil grain size are important factors in determining the kinetics of soil carbonate formation and interpreting the resulting isotopic record.

2. BACKGROUND

2.1. Carbonate formation in cold-climate soils and sub-glacial environments

Pedogenic carbonates are common in cold climates (Lacelle, 2007), and have been identified at high latitude in the Arctic (Swett, 1974; Bunting and Christensen, 1978; Forman and Miller, 1984; Mann et al., 1986; Marlin et al., 1993; Courty et al., 1994; Kabala and Zapart, 2012) and Antarctic (Tedrow and Ugolini, 1966; McCraw, 1967; Vogt and Corte, 1996; Campbell and Claridge, 1998; Foley, 2005), as well as at high elevation sites (Quade et al., 2007, 2011, 2013; Hoke et al., 2009; Burgener et al., 2016). In this study, we define a "cold climate" site as one having at least two consecutive months where mean monthly air or soil temperatures are less than or equal to $0\,°C$. Carbonates from such cold climates are considered "cryogenic" when their precipitation is driven by the freezing of a calcium bicarbonate soil solution, which increases ion concentrations in the residual solution and leads to $CaCO_3$ supersaturation (Hallet, 1976; Marlin et al., 1993; Courty et al., 1994; Vogt and Corte, 1996). Cryogenic soil carbonates typically form as pendants on the underside of coarse clasts embedded in the soil matrix. They form because carbonate-bearing soil water accumulates on the underside of clasts due to gravity and is retained there by surface tension; and subsequent freezing of the soil water leads to calcium carbonate supersaturation and carbonate precipitation (Courty et al., 1994). In addition to this cryogenic carbonate formation process, soil carbonate formation in cold climates can also occur via "normal" processes common in temperate and warm soils, involving supersaturation of a soil solution due to soil drying or CO_2 outgassing (see Breecker et al., 2009 for more detail). Unlike the cryogenic soil carbonates, these "normal" soil carbonates are thought to form under conditions of near-isotopic equilibrium, and may exhibit seasonal biases in their isotopic composition depending on individual soil characteristics (Breecker et al., 2009; Peters et al., 2013; Hough et al., 2014; Burgener et al., 2016; Ringham et al., 2016; Gallagher and Sheldon, 2016).

In contrast to pedogenic carbonates, which can potentially form in any soil that experiences suitable climate conditions, the occurrence of cryogenic sub-glacial carbonates is limited to areas of present or past glaciation. Sub-glacial carbonate precipitation is induced by pressure melting on the uphill (stoss) side of topographic bed obstacles, and subsequent refreezing on the downhill (lee) side of the obstacle (Hanshaw and Hallet, 1978; Souchez and Lemmens, 1985). As the water refreezes on the lee side of the obstacle, ions are excluded from the ice and concentrated in the remaining solution, until the solution reaches calcite supersaturation and calcite precipitation begins (Fig. 2); (Hallet, 1976; Hanshaw and Hallet, 1978; Souchez and Lemmens, 1985).

2.2. Non-equilibrium processes in cryogenic carbonates

There is an extensive body of literature investigating the various kinetic processes causing disequilibrium effects in
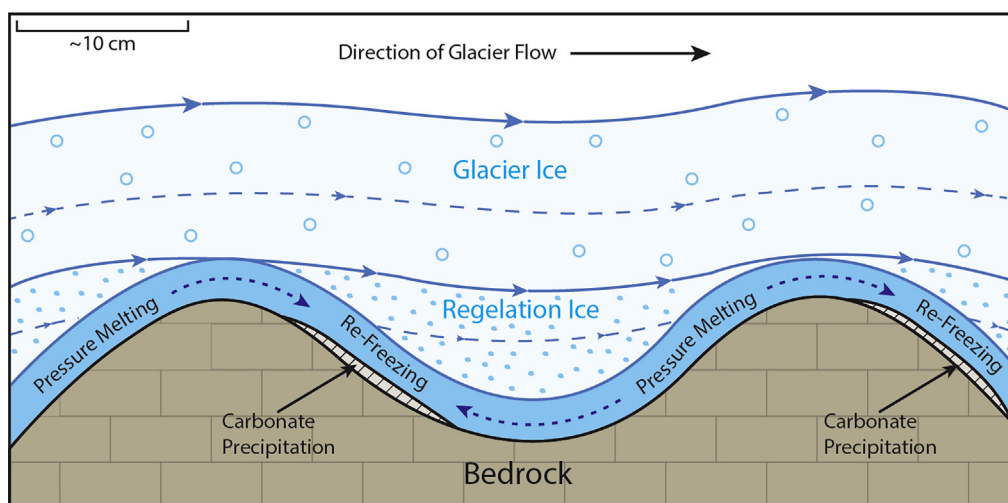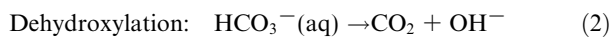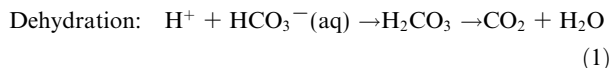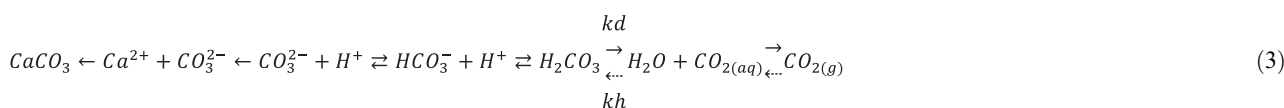

Fig. 2. Schematic representation of carbonate precipitation in sub-glacial environments. Modified from Hanshaw and Hallet (1978).

carbonate clumped and conventional stable isotopic compositions (e.g., Clark and Lauriol, 1992; Zeebe and Wolfe-Gladrow, 2001; Watson, 2004; Ghosh et al., 2006; Dietzel et al., 2009; Guo, 2009; Lachniet, 2009; Watson and Müller, 2009; Dennis and Schrag, 2010; Tripati et al., 2010, 2015; Daëron et al., 2011; DePaolo, 2011; Gabitov et al., 2012; Kluge and Affek, 2012; Saenger et al., 2012; Wang et al., 2013; Watkins et al., 2013, 2014; Affek et al., 2014; Affek and Zaarur, 2014; Kluge et al., 2014; Watkins and Hunt, 2015; Devriendt et al., 2017). The schematic diagram in Fig. 3 (modified after Tripati et al., 2015) summarizes the expected effects of the most relevant of these disequilibrium processes on carbonate Δ_{47}, $\delta^{18}O$, and $\delta^{13}C$ values. As discussed in the following sections, the pri-

Dehydration: $H^+ + HCO_3^-(aq) \rightarrow H_2CO_3 \rightarrow CO_2 + H_2O$

$$(1)$$

Dehydroxylation: $HCO_3^-(aq) \rightarrow CO_2 + OH^-$ (2)

Bicarbonate dehydration is the dominant CO_2 degassing reaction at typical soil pH levels, and will thus be the focus of this discussion (Guo, 2009). Various studies have shown that kinetic isotope fractionations occur during bicarbonate dehydration (Marlier and O'Leary, 1984; Paneth and O'Leary, 1985; Clark and Lauriol, 1992; Zeebe and Wolfe-Gladrow, 2001; Guo, 2009; Affek and Zaarur, 2014; Tripati et al., 2015). Clark and Lauriol (1992) and Guo (2009) describe the following schematic reaction pathway between calcium carbonate and gaseous CO_2:

$$CaCO_3 \leftarrow Ca^{2+} + CO_3^{2-} \leftarrow CO_3^{2-} + H^+ \rightleftarrows HCO_3^- + H^+ \rightleftarrows H_2CO_3 \underset{\leftarrow\cdots}{\overset{kd}{\rightarrow}} H_2O + CO_{2(aq)} \underset{\leftarrow\cdots}{\overset{\rightarrow}{}} CO_{2(g)} \qquad (3)$$

(below the equation: kh)

mary disequilibrium processes associated with cryogenic carbonate formation are CO_2 degassing via bicarbonate dehydration, and pH-related effects.

2.2.1. CO$_2$ degassing via bicarbonate dehydration and dehydroxylation

Outgassing of CO_2 implies removal of dissolved inorganic carbon (DIC) from solution, and yet this process promotes calcium carbonate saturation by increasing the solution pH as well as the concentration of dissolved CO_3^{2-}. Degassing of CO_2 can proceed via two different reactions known as bicarbonate dehydration and dehydroxylation (Clark and Lauriol, 1992; Fairchild et al., 2007; Guo, 2009):
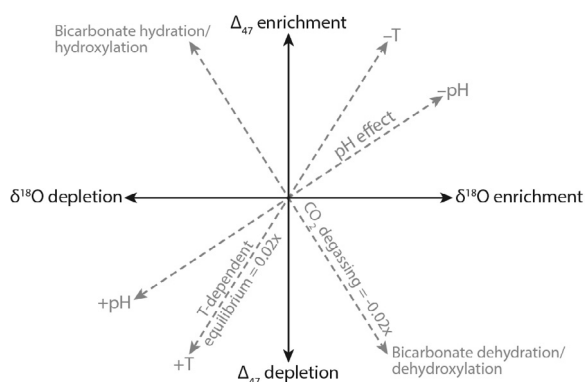

Fig. 3. Schematic illustration of several carbonate equilibrium and disequilibrium fractionation processes and their effects on carbonate Δ_{47} and $\delta^{18}O$. +pH and –pH represent the isotopic effects of increasing or decreasing the pH of a bicarbonate solution, respectively. +T and –T show the isotopic effects of increasing or decreasing the temperature of a bicarbonate solution. Modified from Tripati et al. (2015).

where the dotted arrows indicate reactions that are unimportant during rapid processes, and kd and kh are the rate constants for bicarbonate dehydration and hydration, respectively. When rehydration (kh in the above reaction) is insignificant, degassing of aqueous CO_2 to gaseous CO_2 is quantitative (e.g., all of the reactant is consumed) and non-fractionating (Clark and Lauriol, 1992). The precipitation reaction ($Ca^{2+} + CO_3^{2-} \rightarrow CaCO_3$) can give rise to small kinetic fractionations (<2‰; Watkins et al., 2014) that can partially offset the kinetic fractionations due to bicarbonate dehydration, but which are hereafter neglected due to their relatively small magnitude. Additionally, the equilibrium timescales for the various (de)protonation reactions (e.g., $CO_3^{2-} + H^+ \rightarrow HCO_3^-$; $HCO_3^- + H^+ \rightarrow H_2CO_3$) are several orders of magnitude lower (~10–7 s) than the bicarbonate dehydration reaction (~10 s) (Zeebe and Wolfe-Gladrow, 2001), making the decomposition of carbonic acid ($H_2CO_3 \rightarrow CO_{2(aq)} + H_2O$) the rate limiting step in the reaction pathway, and the control on kinetic isotope fractionations during bicarbonate dehydration. Both Clark and Lauriol (1992) and Guo (2009) found that CO_2 degassing and associated bicarbonate dehydration during the formation of cryogenic carbonate powders results in calcites enriched in ^{18}O and ^{13}C relative to the expected equilibrium isotope composition. Affek and Zaarur (2014) and Tripati et al. (2015) confirmed these findings and showed that bicarbonate dehydration also leads to lower calcite Δ_{47} values (high apparent carbonate formation temperatures) relative to the expected equilibrium Δ_{47} value. Burgener et al. (2016) hypothesized that this bicarbonate dehydration process was responsible for the hotter-than-expected apparent soil carbonate formation temperatures (low Δ_{47} values), and high $\delta^{18}O$ and $\delta^{13}C$ composition in soil carbonates collected at a cold (mean annual soil temperature ~1 °C), high elevation (4700 m) site in north-central Chile.

As shown in the schematic reaction Eq. (3), enrichment in carbonate ^{18}O and ^{13}C values and decreases in Δ_{47} values are due to kinetic isotope fractionations associated with the decomposition of carbonic acid during CO_2 degassing and bicarbonate dehydration. With respect to carbonate ^{18}O and ^{13}C, enrichment occurs because $^{12}C-O$ and $C-^{16}O$ bonds are preferentially broken over $^{13}C-O$ and $C-^{18}O$ bonds during H_2CO_3 decomposition, resulting in lower $\delta^{18}O$ and $\delta^{13}C$ values for the CO_2 gas and higher $\delta^{18}O$ and $\delta^{13}C$ values for the residual HCO_3^- pool (Clark and Lauriol, 1992). The high $\delta^{18}O$ and $\delta^{13}C$ DIC composition is then inherited by the precipitating calcite. The decrease in Δ_{47} values (reflecting depletion in the abundance of calcite CO_3^{2-} groups containing both ^{13}C and ^{18}O) occurs because degassing CO_2 from a bicarbonate solution acts as a non-linear, "reverse" mixing reaction (Eiler and Schauble, 2004). In a forward mixing reaction, if two populations of CO_2 (or HCO_3^-) with identical Δ_{47} compositions but unique $\delta^{13}C$ and $\delta^{18}O$ compositions are mixed together, the resulting mixed population will have a new Δ_{47} composition that is a non-linear combination of the two end-member populations (Defliese and Lohmann, 2015). In contrast, the separation of a carbon pool (the degassed CO_2) with a distinct bulk $\delta^{18}O$ and $\delta^{13}C$ composition from the original carbon reservoir (the initial DIC pool) is essentially the reverse of the "forward" mixing reactions described by Eiler and Schauble (2004), and results in a final carbon pool (the remnant DIC pool) with a new bulk isotope composition and a Δ_{47} composition that is not a linear (e.g., mass balanced) product of the separated carbon pool and original reservoir (Guo, 2009). Guo (2009) modeled the kinetic isotope fractionations associated with bicarbonate dehydration, and predicted that at 0 °C, for every 1‰ increase in calcite $\delta^{18}O$, there should be a corresponding 1.1–3.2‰ increase in $\delta^{13}C$ and a 0.02–0.027‰ decrease in Δ_{47}. In contrast, empirical data from cryogenic carbonate powders collected from several caves in northwestern Germany show a $0.005 \pm 0.003‰$ decrease in Δ_{47} for every 1‰ increase in calcite $\delta^{18}O$ (Kluge et al., 2014), suggesting that either the Guo (2009) kinetic fractionation model is not completely correct, or that there may be some variability in the relationship between $\delta^{18}O$ enrichment and Δ_{47} depletion in natural carbonates.

2.2.2. pH effect

The equilibrium oxygen and clumped isotope composition of a carbonate is expected to be independent of pH; however under disequilibrium conditions pH affects the oxygen and clumped isotope composition of precipitating calcite (Hill et al., 2014; Watkins et al., 2014). The pH of a carbonate solution controls the relative abundance of the various DIC species ($CO_{2(aq)}$, CO_3^{2-}, HCO_3^-) and each of these DIC species has a distinct equilibrium clumped and stable isotope composition (Usdowski and Hoefs, 1993; Zeebe, 1999, 2007; Beck et al., 2005; Tripati et al., 2010; Hill et al., 2014; Tripati et al., 2015). At a given pH, the isotopic composition of the DIC pool will be the weighted sum of the various DIC species. For calcite grown slowly, under near equilibrium conditions, the oxygen isotope fractionation between calcite and water is independent of the oxygen isotope composition of the DIC pool. Additionally, slowly-forming carbonate has time to reach a state of bulk isotopic equilibrium (e.g., isotopic equilibrium between the crystal surface boundary layer and interior crystal lattice), leading to a Δ_{47} value that depends only on the temperature of the formation water (Watson and Müller, 2009; Tripati et al., 2010; Hill et al., 2014). However, if carbonate precipitation occurs at a sufficiently high rate, the carbonate mineral will incorporate the Δ_{47} signature of the DIC pool (Hill et al., 2014). Under such rapid growth conditions, higher pH values will lead to lower ^{18}O and Δ_{47} values compared to the expected equilibrium calcite composition (Fig. 3; Tripati et al., 2010, 2015; Hill et al., 2014; Watkins et al., 2014; Watkins and Hunt, 2015).

Due to the temperature dependence of the equilibration rates between the DIC pool and water (with respect to oxygen isotopes) and the DIC pool and precipitating calcite (with respect to carbon isotopes), carbonates forming in cold environments are thought to be more susceptible to KIEs (Clark and Lauriol, 1992; Tripati et al., 2010). The time required for the DIC pool to reach isotopic equilibrium for both ^{13}C and ^{18}O is much longer at 0 °C than at 25 °C. For ^{13}C, the DIC equilibration time is approximately 24 s at 25 °C, and 440 s at 0 °C (Zeebe et al., 1999; Clark and Lauriol, 1992). The DIC equilibration times for ^{18}O are much slower, in the range of ∼1 to 9 h at 25 °C, and ∼6 to 150 h at 0 °C over the normal range of soil pHs (Uchikawa and Zeebe, 2012). Based on these considerations, Tripati et al. (2010) suggested that disequilibrium processes like bicarbonate dehydration are more likely to produce isotopic disequilibrium in carbonates forming in cold environments than in temperate environments, because at cold temperatures (e.g., near freezing) carbonate precipitation may proceed more rapidly than isotopic equilibration in the DIC pool (see also Clark and Lauriol, 1992).

By sampling modern/Holocene soil carbonates from cold environments at high latitude and elevation, as well as sub-glacial carbonates, we explore potential disequilibrium processes during cryogenic carbonate formation, and investigate how varying soil environment characteristics (e.g., soil moisture, sediment grain size, etc.) affect the magnitude of any observed KIE.

3. METHODS

We collected cold-environment soil carbonates from the Dry Valleys, Antarctica; Svalbard, Norway, in the High Arctic; the Chilean and Argentinian Andes; and Tibetan plateau, China; as well as sub-glacial carbonates from Montana, USA and British Colombia, Canada (Table 1). Sample analyses included Δ_{47}, $\delta^{18}O$, and $\delta^{13}C$ measurements of soil and sub-glacial carbonate, and XRD to determine mineralogy for select samples suspected of dolomite contamination. Context was established for the sample data using meteorological data and in-situ measurements of soil and sub-glacial conditions, as described in the following section.

Table 1
Sample location and environmental conditions.

Sample name	Study Site	Latitude (°N)	Longitude (°E)	Elevation (m)	Depth in soil (cm)	Age	Environment	Sample Source	Data Source	
									Clumped Isotopes	Stable Isotopes
Soil carbonates										
Elq13-4700-20	Elqui Valley, Chile	−30.177	−69.829	4700	20	345 ± 30[b]	High Elevation Desert	Burgener et al. (2016)	Burgener et al. (2016)[a]	Burgener et al. (2016)
Elq13-4700-40	Elqui Valley, Chile	−30.177	−69.829	4700	40	345 ± 30[b]	High Elevation Desert	Burgener et al. (2016)	Burgener et al. (2016)[a]	Burgener et al. (2016)
Elq13-4700-60	Elqui Valley, Chile	−30.177	−69.829	4700	60	345 ± 30[b]	High Elevation Desert	Burgener et al. (2016)	Burgener et al. (2016)[a]	Burgener et al. (2016)
Elq13-4700-80	Elqui Valley, Chile	−30.177	−69.829	4700	80	345 ± 30[b]	High Elevation Desert	Burgener et al. (2016)	Burgener et al. (2016)[a]	Burgener et al. (2016)
Elq13-4700-100	Elqui Valley, Chile	−30.177	−69.829	4700	100	345 ± 30[b,c]	High Elevation Desert	Burgener et al. (2016)	Burgener et al. (2016)[a]	Burgener et al. (2016)
Elq13-4500-50	Elqui Valley, Chile	−30.138	−69.830	4500	50	NA	High Elevation Desert	Burgener et al. (2016)	Burgener et al. (2016)[a]	Burgener et al. (2016)
Elq13-4200-50	Elqui Valley, Chile	−30.164	−69.862	4200	50	9663 ± 40[b]	High Elevation Desert	Burgener et al. (2016)	Burgener et al. (2016)[a]	Burgener et al. (2016)
Elq13-3750-50	Elqui Valley, Chile	−30.206	−69.916	3750	50	2336 ± 30[b]	High Elevation Desert	Burgener et al. (2016)	Burgener et al. (2016)[a]	Burgener et al. (2016)
Elq13-3550-20	Elqui Valley, Chile	−30.262	−69.942	3550	20	5780 ± 30[b,c]	High Elevation Desert	Burgener et al. (2016)	Burgener et al. (2016)[a]	Burgener et al. (2016)
Peters-B15	Río Mendoza Valley, Argentina	−32.812	−70.064	3200	15	Holocene	Arid	Peters et al. (2013)	Peters et al. (2013)	Peters et al. (2013)
Peters-B30	Río Mendoza Valley, Argentina	−32.812	−70.064	3200	30	Holocene	Arid	Peters et al. (2013)	Peters et al. (2013)	Peters et al. (2013)
Peters-B45	Río Mendoza Valley, Argentina	−32.812	−70.064	3200	45	Holocene	Arid	Peters et al. (2013)	Peters et al. (2013)	Peters et al. (2013)
Ant-1	Scott Base, Antarctica	−77.849	166.768	<10	Surface	<12,000	Polar Desert	This Study	This Study	This Study
Ant-2	Victoria Valley, Antarctica	−77.377	161.814	361	Surface	<12,000	Polar Desert	This Study	This Study	This Study
Ant-3	Victoria Valley, Antarctica	−77.377	161.814	361	Surface	<12,000	Polar Desert	This Study	This Study	This Study
Ant-4	Victoria Valley, Antarctica	−77.377	161.814	361	Surface	<12,000	Polar Desert	This Study	This Study	This Study

Table 1 (*continued*)

Sample name	Study Site	Latitude (°N)	Longitude (°E)	Elevation (m)	Depth in soil (cm)	Age	Environment	Sample Source	Data Source	
									Clumped Isotopes	Stable Isotopes
Tsangpo-19	Tibet	30.418	82.767	4800	110	Early Holocene to Latest Pleistocene[d]	Semi-Arid	Quade et al. (2011)	This Study	This Study
Tsangpo-21a	Tibet	29.204	88.309	4016	60	Early Holocene to Latest Pleistocene[d]	Semi-Arid	Quade et al. (2011)	This Study	This Study
Tsangpo-21b	Tibet	29.204	88.309	4016	60	Early Holocene to Latest Pleistocene[d]	Semi-Arid	Quade et al. (2011)	This Study	This Study
Tsangpo-22	Tibet (near Shigatse)	29.317	88.942	3876	55	<5000[d]	Semi-Arid	Quade et al. (2011)	This Study	This Study
Lhasa-4	Tibet (near Lhasa)	29.636	91.292	3809	60	Early Holocene to Latest Pleistocene[d]	Semi-Arid	Quade et al. (2011)	This Study	This Study
Cannes-62	Cannes, Spitsbergen, Svalbard	78.937	11.455	60	62	11,750 ± 430[b]	Polar Desert	Courty et al. (1994), Mann et al. (1986)	This Study	This Study
KG-201a	Arrigetch, Spitsbergen, Svalbard	79.010	11.982	<10	Unknown	9440 ± 360 to 10,000 ± 170[b]	Vegetated	Courty et al. (1994) Mann et al. (1986)	This Study	This Study
KG-201b	Arrigetch, Spitsbergen, Svalbard	79.010	11.982	<10	Unknown	9440 ± 360 to 10,000 ± 170[b]	Vegetated	Courty et al. (1994), Mann et al. (1986)	This Study	This Study
Sub-glacial carbonates										
CG-1	Castleguard Glacier, British Columbia	52.080	−117.269	2100	–	NA	Sub-Glacial	This Study	This Study	This Study
CG-2	Castleguard Glacier, British Columbia	52.080	−117.269	2100	–	NA	Sub-Glacial	This Study	This Study	This Study
BF-1	Blackfoot Glacier, Montana	48.605	−113.662	2000	–	NA	Sub-Glacial	Hanshaw and Hallet (1978)	This Study	This Study
BF-2	Blackfoot Glacier, Montana	48.605	−113.662	2000	–	NA	Sub-Glacial	Hanshaw and Hallet (1978)	This Study	This Study
BF-3	Blackfoot Glacier, Montana	48.605	−113.662	2000	–	NA	Sub-Glacial	Hanshaw and Halle (1978)	This Study	This Study

[a] Δ_{47} values recalculated using Brand et al. (2010) parameters, following Daëron et al. (2016) and Schauer et al. (2016).
[b] Radiocarbon age (BP).
[c] Measured on a separate soil carbonate sample from the same soil profile.
[d] Age estimated from Gile et al. (1966) definition of Stage I, II, and III soil carbonates.

3.1. Field methods and sampling procedures

Soil carbonate samples were collected from sixteen Early Holocene to recent sites representing a range of cold-climate soils and two sub-glacial sites (Table 1) by different research groups using similar sampling methods at each soil site. In order to ensure that the sampled carbonates had formed *in situ*, care was taken at each soil site to collect only carbonate pendants that were found on the underside of *in situ* clasts (e.g., Burgener et al., 2016). Sampling methods and meterological data for each site are described in the following paragraphs and summarized in Table 2.

The quality of soil temperature, soil moisture, and water $\delta^{18}O$ estimates varies from site to site due to a variety of factors, including the type of water sample collected, the distance between the meteorological stations and our soil sampling sites, and the temporal resolution of the dataset. For example, the meteoric water $\delta^{18}O$ data for the Svalbard sites comes from a Global Network of Isotopes in Precipitation (GNIP) station with nearly continuous measurements from 1990 to 2015, but the station (World Meteorological Organization [WMO] code: 100400) is located several kilometers away from the sample sites. In contrast, water $\delta^{18}O$ data for the Tsangpo-19 site was collected at the sample site, but comes from a limited number of individual samples collected by hand from local streams and snowpack.

At the two Antarctic soil sites, soil carbonate pendants were collected in 2015 as samples of opportunity from surficial, non-carbonate clasts. Scott Base soils are characterized by a weakly weathered, angular basaltic ash matrix dominated by gravel- to sand-sized particles, while soils in Victoria Valley are composed of weakly weathered sand and gravel that are ice-cemented below 40 cm, and capped by a 2 cm-thick, desert pavement (Hagedorn et al., 2010; see Supplementary Information Section 2). Snow, ice, and water samples were collected from Victoria Valley and their isotopic values analyzed as part of an earlier study (see Hagedorn et al., 2010, Section 2).

For the Chilean and Argentinian Andes samples, soil carbonate pendants and local snow, rain, and stream water samples were collected between 2009 and 2013 near the international border between Chile and Argentina (Peters et al., 2013; Burgener et al. (2016)). The Chilean samples include carbonates collected at 20, 40, 60, 80, and 100 cm depths at 4700 masl, samples collected at 50 cm depths for the 3750, 4200, and 4500 masl profiles, and a sample collected 20 cm below the ground surface from the 3550 masl profile (see Burgener et al. (2016), Section 3). For the Argentinian samples collected by Peters et al. (2013), only the upper 50 cm of the 3200 masl soil site experiences at least two consecutive months of sub-zero temperatures; thus, only the three samples collected between 15 and 45 cm depth are included in this study (see Peters et al. (2013), Section 3.1). For both the Chilean and Argentinian samples, carbonate pendants on non-carbonate clasts were collected every 20 cm from the soil surface down to 1 m depth. The Chilean 4700 masl sample site is completely devoid of vegetation and is located less than 100 m from two small, perennial ice fields. The upper 100 cm of the

local soil is composed of unconsolidated clasts with a mean diameter of ~3 cm (Burgener et al., 2016). In contrast, the 3550, 3750, 4200, and 4500 masl soil pits are located along small, upper tributaries of the Elqui River, and are composed of a consolidated, clast-supported conglomerate with a sandy inter-cobble soil matrix. The Argentinian 3200 masl soil was covered with relatively abundant vegetation and composed of much more fine-grained sediments (predominantly silt with thin mud and fine sand horizons). Both the Chilean and Argentinian samples were previously analyzed and their clumped and stable isotope compositions reported by Burgener et al. (2016) and Peters et al. (2013), respectively. The Burgener et al. (2016) samples were not re-analyzed for this study, but their Δ_{47} values were re-calculated using the ^{17}O correction parameters of Brand et al. (2010), following the recommendations of Daëron et al. (2016) and Schauer et al. (2016), and the T (Δ_{47}) values were recalculated using the T-Δ_{47} calibration of Kelson et al. (2017) (see Section 4.3). Due to a lack of material from the 3200 masl site, the Peters et al. (2013) samples could not be reanalyzed. Additionally, because these samples were analyzed at a different laboratory (Caltech) using older methods and T-Δ_{47} calibrations, their Δ_{47} and T(Δ_{47}) values could not be recalculated using modern methods. However, material collected at a lower elevation site in the Río Mendoza Valley was reanalyzed using the methods described in Section 3.4 of this paper and yielded similar results to the original Peters et al. (2013) values, suggesting that the Δ_{47}, $\delta^{18}O$, and $\delta^{13}C$ values of the Argentinian Andes samples are directly comparable to the new results reported in this study.

Quade et al. (2011, 2013) collected soil carbonate pendants and water, snow, and ice samples from multiple locations across the southern Tibetan Plateau (Fig. 1C). The carbonate pendant samples re-analyzed in this study were collected at a variety of depths from three soil profiles along the Yarlung Tsangpo valley, and from one soil profile near Lhasa, Tibet (Table 1). The Tsangpo soils are characterized by significant loess deposits that either overlie or are incorporated into the soils. Minor gravels are common, but the soil is dominated by silt to sand-sized particles. The parent material for the Tsangpo-21 soil profile is calcareous sandstone and moderately calcareous siltstone; the parent material at the other three Tsangpo sites is non-calcareous. The uppermost horizon of the Lhasa soil is a ~0.75 m thick angular conglomerate that overlies a 1.5 m loess deposit. Clumped isotope analyses were conducted on some of these samples at the California Institute of Technology using early methodologies (Quade et al., 2011, 2013); to ensure consistency with the other datasets in this study, we reanalyzed the samples following the methods described in Section 3.3.

For the High Arctic samples, soil carbonate pendants were collected in the mid-1980s from two sites at Cannes and Kapp Guissez, near Ny-Ålesund, Svalbard, Norway (Fig. 1B). The Cannes soil is characterized by a "polar desert" environment with less than 10% plant cover, while the Kapp Guissez soil site is characterized by 100% plant cover (Mann et al., 1986). The Cannes polar desert soil exhibits a well-developed, coarsening-upwards desert pavement

Table 2
Temperature, $\delta^{18}O$, and Δ_{47} assumptions for each sample site.

Study sites	Expected carbonate precipitation temperatures (°C)[a]			Temperature type	References	Expected surface water $\delta^{18}O$ (VSMOW)		References	Expected equilibrium carbonate Δ_{47} value (‰)[h]		
	Min	MST	WMMT			Min	Max		−1 °C	MST	WMMT
Elqui Valley, Chile 4700 m (10 cm)	−1	9	10	Soil	Burgener et al. (2016)	−20	−15	Burgener et al. (2016)	0.7336	0.6325	0.6289
Elqui Valley, Chile 4700 m (50 cm)	−1	7	9	Soil	Burgener et al. (2016)	−20	−15	Burgener et al. (2016)	0.7336	0.6398	0.6325
Elqui Valley, Chile 4500 m (50 cm)	−1	9	11	Soil	Burgener et al. (2016)[b]	−20	−15	Burgener et al. (2016)	0.7336	0.6325	0.6254
Elqui Valley, Chile 4200 m (50 cm)	−1	11	13	Soil	Burgener et al. (2016)[b]	−17	−15	Burgener et al. (2016)	0.7336	0.6254	0.6184
Elqui Valley, Chile 3750 m (50 cm)	−1	14	16	Soil	Burgener et al. (2016)[b]	−16	−14	Burgener et al. (2016)	0.7336	0.6150	0.6082
Elqui Valley, Chile 3550 m (10 cm)	−1	16	16	Soil	Burgener et al. (2016)	−15	−12	Burgener et al. (2016)	0.7336	0.6082	0.6082
Las Cuevas, Río Mendoza Valley, Argentina (10 cm)	−1	15	17	Soil	Peters et al. (2013)[c]	−17	−9	Hoke et al. (2009)	0.7828	0.7033	0.6938
Las Cuevas, Río Mendoza Valley, Argentina (30 cm)	−1	14	17	Soil	Peters et al. (2013)[c]	−17	−9	Hoke et al. (2009)	0.7828	0.7082	0.6938
Las Cuevas, Río Mendoza Valley, Argentina (50 cm)	−1	14	16	Soil	Peters et al. (2013)[c]	−17	−9	Hoke et al. (2009)	0.7828	0.7082	0.6985
Scott Base, Antarctica	−1	−1	2	Soil	NRCS Weather Station[d]	−33	−29	Hagedorn et al. (2010)	0.7336	0.6705	0.6586
Victoria Valley, Antarctica	−1	0	3	Soil	NRCS Weather Station[d]	−33	−29	Hagedorn et al. (2010)	0.7336	0.6665	0.6548
Svalbard	−1	3	5	Soil	Mann et al., 1986; GTNP data repository[e]	−14	−8	GNIP[g]	0.7336	0.6548	0.6472
Lhasa, Tibet	−1	18	19	Air	Quade et al., 2013; ISD repository[f]	−14	−12	GNIP[g]	0.7336	0.6016	0.5983
Tsangpo Site 19, Tibet	−1	13	15	Air	Quade et al. (2013); ISD repository[f]	−17	−15	Quade et al. (2011)	0.7336	0.6184	0.6116
Tsangpo Site 21, Tibet	−1	15	15	Air	ISD repository[f]	−19	−16	Quade et al. (2011)	0.7336	0.6116	0.6116
Tsangpo Site 22, Tibet	−1	15	15	Air	ISD repository[f]	−18	−17	Quade et al. (2011)	0.7336	0.6116	0.6116
Castleguard Glacier	−1	0	0	Meltwater	This Study	−20	−19	Hitchon and Krouse (1972)	0.7336	0.6665	0.6665
Blackfoot Glacier	−1	0	0	Meltwater	Hanshaw and Hallet (1978)	−15	−14	Hanshaw and Hallet (1978)	0.7336	0.6665	0.6665

[a] Except where indicated, carbonate precipitation temperatures are calculated for −1 °C (minimum possible precipitation temperature), mean summer temperature (MST), and warmest mean monthly soil or air temperature (WMMT).
[b] Soil temperatures interpolated from Burgener et al. (2016) 4700 and 3550 masl station data.
[c] 30 cm soil temperature interpolated from Peters et al. (2013) 10 and 50 cm data.
[d] Data from USDA Natural Resources Conservation Services Program weatherstations.
[e] Data from the Global Terrestrial Network for Permafrost database (http://www.gtnpdatabase.org).
[f] Data from the Integrated Surface Database repository (ftp://ftp.ncdc.noaa.gov/pub/data/noaa/).
[g] Global Network of Isotopes in Precipitation (GNIP), Lhasa Station (http://www-naweb.iaea.org/napc/ih/IHS_resources_gnip.html).
[h] All samples but Peters et al. (2013) samples calculated using Kelson et al. (2017) T-Δ_{47} calibration and the expected carbonate precipitation temperatures at each site. Peters et al. (2013) samples calculated using Ghosh et al. (2006) T-$\Delta 47$ calibration.

composed of angular pebbles and pedogenic silt accumulations, which overlies a weakly developed A horizon and a Bk horizon characterized by dolomitic silt accumulation and calcite pendants on the undersides of rocky clasts (Mann et al., 1986). In contrast, the vegetated Kapp Guissez soils are characterized by a lack of a desert pavement, and a well-developed O or A horizon overlying a Bk horizon with much thinner silt accumulations (Mann et al., 1986). The pendant samples from the Cannes site formed on dolomitic clasts, while the sample from Kapp Guissez formed on a non-carbonate igneous cobble. Due to the high concentration of dolomitic sediment in the Cannes profile (Mann et al., 1986), the mineral composition of the Cannes samples was determined by x-ray diffraction (XRD).

The sub-glacial carbonates analyzed in this study were collected at two sites: (1) Blackfoot Glacier, located in Glacier National Park in northwest Montana, and (2) Castleguard Glacier, in the Columbia Icefield ∼160 km northwest of Banff, Alberta. Hanshaw and Hallet (1978) collected sub-glacial carbonate samples for stable oxygen and carbon isotope analysis from the surface of carbonaceous bedrock that had been recently exposed by the retreat of the Blackfoot Glacier in northwest Montana, USA, as well as meltwater and ice samples. The carbonate samples were reanalyzed for this study to determine their $\delta^{18}O$, $\delta^{13}C$, and Δ_{47} compositions. Samples from similar bedrock exposures at Castleguard Glacier, British Columbia, Canada were collected by the same researchers following the same methods, and the $\delta^{18}O$, $\delta^{13}C$, and Δ_{47} values for these samples are reported here for the first time.

Details regarding the sources of weather station air and soil monitoring data and meteoric water $\delta^{18}O$ values are described in the online Supplementary Information.

3.2. X-Ray diffraction methods

The soil carbonate pendant samples from the Arctic Cannes site in Svalbard formed on the underside of dolomitic clasts (Mann et al., 1986). To assess whether detrital carbonate that had been incorporated into the pedogenic pendant was inadvertently sampled, the mineral composition of the carbonate pendant sample was determined via x-ray diffraction at the University of Washington's Materials Science and Engineering User Facility in the Department of Materials Science and Engineering. X-ray diffraction patterns were acquired using a Bruker D8 Focus Bragg-Brentano powder diffractometer with a scintillator-type detector and nickel filter, operating at 40 kV and 40 mA with a Cu-Kα radiation source of 1.54 Å. Scan data were collected between 20 and 90° 2θ with a 0.02°step size.

3.3. Clumped and stable isotope analysis laboratory methods

Clumped isotope analyses ($\delta^{18}O$, $\delta^{13}C$ and Δ_{47}) were conducted at the University of Washington's IsoLab following the methods of Burgener et al. (2016) and Kelson et al. (2017). In summary, 6–8 mg of each carbonate sample was digested in a common bath of phosphoric acid held at 90 °C and with an initial specific gravity of 1.904–1.970 g cm^3. The evolved CO_2 was cryogenically separated from water

on an automated stainless steel and nickel vacuum line using an ethanol-dry ice slush trap, isolated in a liquid N_2 trap, and passed through a Porapaq Q trap using He as the carrier gas. Every 4–5 carbonate sample unknowns, a carbonate standard (intralaboratory standards: C64, C2, Coral; and interlaboratory standards ETH1, ETH2, ETH3 and ETH4; mean $\delta^{18}O$, $\delta^{13}C$ and Δ_{47} values for these standards are reported in Table SI1) was purified on the vacuum line and transferred into a Pyrex break seal. Sample and standard break seals were then loaded into an automated 10-port tube cracker inlet system on a Thermo MAT 253 configured to measure m/z 44–49 inclusive.

Δ_{47}, $\delta^{13}C$, and $\delta^{18}O$ values were calculated for all samples following the methods of Huntington et al. (2009) with updated methods for (1) pressure baseline (PBL) measurement (He et al., 2012); (2) $\delta^{13}C$ value correction for ^{17}O interference using the parameters described in Brand et al. (2010), following the methods of Daëron et al. (2016) and Schauer et al. (2016); and (3) Δ_{47} correction to the Absolute Reference Frame (ARF) using heated gas and CO_2-water equilibration lines constructed during the corresponding analysis period (Dennis et al., 2011). Scripts for these calculations are provided by Schauer et al. (2016). $\delta^{13}C$ was referenced to the international standards NBS-19 and LSVEC, and $\delta^{18}O$ was referenced to NBS-18 and NBS-19. Samples with Δ_{48} values higher than 2‰, indicating contamination, were rejected. Following Ross (2003) and Zaarur et al. (2013), the Pierce outlier test was used to identify and remove statistical outliers (n = 4) in the Δ_{47}, $\delta^{18}O$, and $\delta^{13}C$ values for each of the samples.

3.4. Calculating Δ_{47}, $\delta^{18}O$, and $\delta^{13}C$ anomalies

We use the following methods to compare Δ_{47}, $\delta^{18}O$, and $\delta^{13}C$ observations to expected values for the environments of sample carbonate formation. For the purposes of this study we define the Δ_{47}, and $\delta^{18}O$ anomalies as the observed carbonate Δ_{47} and $\delta^{18}O$ values minus the expected equilibrium carbonate Δ_{47} and $\delta^{18}O$ values. Using this calculation, negative Δ_{47} and $\delta^{18}O$ anomalies show isotopic depletion with respect to the expected equilibrium carbonate composition, while positive anomalies show isotopic enrichment. In contrast to the Δ_{47} and $\delta^{18}O$ anomalies, exact $\delta^{13}C$ anomalies are difficult to calculate due to the lack of direct isotopic measurements of soil CO_2 at our study sites. Instead, we compare the soil carbonate $\delta^{13}C$ values to the expected range of soil CO_2 $\delta^{13}C$ compositions.

Expected equilibrium carbonate Δ_{47} compositions are calculated for different temperatures selected to characterize the likely range of expected carbonate formation temperatures at each site. The minimum expected temperature of carbonate formation for all sites is taken to be −1 °C because carbonate precipitation requires the presence of liquid water, but high salinity solutions such as may be found in sub-glacial environments or hyper-arid soils can have a depressed freezing point. At the sub-glacial sites, the maximum carbonate formation temperature is assumed to be 0 °C. For soil carbonates, the warmest mean monthly air or soil temperature (WMMT or WMMST, respectively) is taken to characterize the maximum likely temperature of

carbonate formation, and expected equilibrium carbonate Δ_{47} compositions are also calculated for local mean summer air or soil temperatures (MST or MSST, respectively). Local WMMT/WMMST and MST/MSST are calculated at each site from available meteorological records (see Table 2). Expected temperatures, expected equilibrium carbonate Δ_{47} compositions corresponding to these assumed formation temperatures are calculated using Eq. (1) in Kelson et al. (2017):

$$\Delta_{47} = 0.0417 \pm 0.0013 \times 10^6/T^2 + 0.139 \pm 0.014 \quad (4)$$

where T is the carbonate formation temperature in Kelvin. The expected equilibrium carbonate Δ_{47} compositions are calculated using the Kelson T-Δ_{47} calibration. This calibration is most appropriate for our samples because the methodologies of Kelson et al. (2017) are the same as this study (90 °C acid digestion, purification apparatus, mass spectrometry including pressure baseline measurements, use of updated ^{17}O correction parameters, etc.). The Kelson T-Δ_{47} calibration is based on a larger sample size (n = 56) than previously published T-Δ_{47} calibrations, and is not different from other published calibration data that have been calculated using the updated ^{17}O correction (Kelson et al., 2017).

Expected equilibrium carbonate $\delta^{18}O$ values are calculated from local minimum and maximum expected carbonate formation temperatures (as described above) and local meteoric water $\delta^{18}O$ values using the temperature-dependent calcite-water oxygen isotope fractionation factor, as defined in Watkins et al. (2014):

$$\Delta^{18}O_{c-w}^{eq} = \frac{17747}{T_K} - 29.777 \quad (5)$$

where $\Delta^{18}O_{c-w}^{eq}$ is equal to the per mil fractionation of oxygen isotopes between water and calcite (equal to $1000 \times \ln(\alpha)$, and T_K is the carbonate formation temperature in Kelvin.

Despite the lack of soil CO_2 $\delta^{13}C$ measurements, general constraints can be placed on expected equilibrium soil carbonate $\delta^{13}C$ values based on the $\delta^{13}C$ composition of the two reservoirs that contribute carbon to soil carbonates: soil CO_2 and atmospheric CO_2. Atmospheric CO_2 is assumed to have ranged between −6.5 (pre-industrial) and −8.5‰ (modern). Soil CO_2 $\delta^{13}C$ is largely determined by the abundance of C3 and C4 plants in the local environment (Cerling and Quade, 1993). The mean $\delta^{13}C$ value of C3 plants (−28.5‰) is more negative than that of C4 plants (−12‰), and thus acts as the lower bound to the expected range of soil CO_2 values (Cerling and Quade, 1993; Kohn, 2010). Because C3 plants are favored in colder, arid to sub-arid environments (Still et al., 2003), we assume that the mean $\delta^{13}C$ value of C3 plants is a reasonable lower bound for expected equilibrium carbonate $\delta^{13}C$ values. To estimate the $\delta^{13}C$ offset from equilibrium (e.g., the approximate $\delta^{13}C$ anomaly) for our samples, we calculated the equilibrium carbonate $\delta^{13}C$ value at carbonate formation temperatures ranging from 0 to 30 °C using the atmospheric and soil CO_2 $\delta^{13}C$ values described above, and the temperature dependent ^{13}C equilibrium fractionation factors for $CO_2(g) - HCO_3^-$ (Mook et al., 1974), $CO_2(aq) - HCO_3^-$

(Mook et al., 1974), and $CO_2(g) - calcite$ (Bottinga, 1968), as summarized in Watkins and Hunt (2015), Table 1. Our measured carbonate $\delta^{13}C$ values are then plotted against this range of expected equilibrium carbonate $\delta^{13}C$ values in order to explore the general relationship between measured and expected values.

4. RESULTS

4.1. Local climate and meteoric water $\delta^{18}O$

4.1.1. Scott base and Victoria Valley, Antarctica

At both Antarctic sites, seasonal soil temperature at depth varies significantly, driven by the annual cycle in air temperature (Table 3, Supplementary Information, and Supplementary Fig. 1). At Scott Base, from 1999 to 2015 (excluding 2008, for which data was not available), MSST at 50 cm depth is −4 °C, and WMMST at the same depth is −2 °C. Near the surface (1 cm depth), MSST at Scott Base is +2 °C. At Victoria Valley, 50 cm MSST from 1999 to 2015 averages −7 °C, and WMMST is −5 °C. MSST at 7 cm depth is −1 °C. The weather station at Victoria Valley weather station failed to record accurate mean annual air temperatures between 1999 and 2015, but did record soil temperatures. Unlike the other soil sites, the samples collected at Scott Base and Victoria Valley were collected from the surface, so the 1 cm (Scott Base) and 7 cm (Victoria Valley) MSST and WMMST values are used to calculate the Δ_{47}, $\delta^{18}O$ anomalies, rather than the 50 cm temperatures.

Soil moisture is extremely low at both Antarctic sites (Supplementary Fig. 1, Table 3), with minima occurring during the winter due to freezing, and maxima occurring during the summer. The $\delta^{18}O$ of the soil water at Victoria Valley varies between −33 (fresh snow) and −29‰ VSMOW (interstitial ice) (Hagedorn et al., 2010). Measurements of the isotopic composition of soil water at Scott Base are unavailable, but are assumed to be similar to the Victoria Valley waters.

4.1.2. Chilean and Argentinian Andes

A soil monitoring station installed by Burgener et al. (2016) at the 4700 masl Elqui Valley, Chile site from January 2014 to January 2015 recorded MSST and WMMST values at 50 cm depth of 7 and 9 °C, respectively. The site is extremely arid, with most precipitation occurring during the winter months; however, soil moisture is highest during the summer months when the past winter's snow begins to melt. During the monitoring period, mean summer soil moisture was 0.08 m^3 m^{-3} and 0.019 m^3 m^{-3} at 10 and 50 cm depth, respectively. At the 3550 masl site, the 50 cm MSST and WMMST over the same period were 15 and 16 °C, respectively, and 50 cm soil moisture was 0.07 m^3 m^{-3}. Burgener et al. (2016) reported $\delta^{18}O$ values ranging from −20 to −15‰ VSMOW for local snow and meltwater at the 4700 masl site, and −15 to −12‰ at the 3550 masl site. Temperature monitoring stations were not installed at the 3750, 4200, and 4500 masl sites; instead, soil temperature for the three sites were interpolated using data from the nearby 3550 and 4700 masl monitoring stations.

Table 3
Weather station location and climatologic data.

Weather Station Location	Lat. (°N)	Lon. (°E)	Elev. (m)	MAT[a] (°C)	MST[b] (°C)	WMMT[c] (°C)	50 cm MAST[d] (°C)	50 cm MSST[e] (°C)	50 cm WMMST[f] (°C)	MAP[g] (mm)	MASM[h] (m³ m⁻³)	Corresponding samples	Distance from sample sites (km)	Reference
Elqui Valley, Chile 4700 m	−30.177	−69.829	4700	NA	NA	NA	0	7	9	89[i]	0.019	Elq13-4700 samples	Same site	Burgener et al. (2016)
Elqui Valley, Chile 3550 m	−30.262	−69.942	3550	5	10	10	8	15	16	89[i]	0.073	Elq13-3550-20	Same site	Burgener et al. (2016)
Río Mendoza Valley, Argentina 3200 m	−32.812	−70.064	3200	NA	NA	NA	8	14	16	NA	0.062	Peters samples	Same site	Peters et al. (2013)
Scott Base, Antarctica	−77.849	166.768	<10	−17	1	5	−18	−4	−2	NA	0.006	Ant-1	<1 km	NRCS Weather Station
Victoria Valley, Antarctica	−77.377	161.814	361	−22	3	12	−22	−7	−5	NA	0.003	Ant-2, Ant-3, Ant-4	<10 km	NRCS Weather Station
Ngangla Ring Tso/ T'u-ko-erh-ho-kung, Tibet	30.55	81.433	4650	4	14	15	NA	NA	NA	640	NA	Tsangpo-19	113/130 km	Quade et al. (2013)/ISD repository
Shigatse, Tibet	29.250	88.883	3880	7	15	15	NA	NA	NA	515	NA	Tsangpo-21a Tsangpo-21b Tsangpo-22	55 km 55 km 10 km	ISD repository
Lhasa, Tibet	29.667	91.133	3800	9	16	17	NA	NA	NA	575	NA	Lhasa	15 km	ISD repository
Ny-Ålesund, Svalbard	78.921	11.833	60	−3	7	9	−3	3	5	385	NA	Cannes Arrigetch	8 km 11 km	Mann et al. (1986); GTNP data repository

[a] Mean Annual Temperature (MAT).
[b] Mean Summer Temperature (MST).
[c] Warmest Mean Monthly Temperature (WMMT).
[d] Mean Annual Soil Temperature (MAST).
[e] Mean Summer Soil Temperature (MSST).
[f] Warmest Mean Monthly Soil Temperature (WMMST).
[g] Mean Annual Precipitation (MAP).
[h] 50 cm Mean Annual Soil Moisture (MASM).
[i] MAP record from nearby station located at 3200 masl.

At the Argentinian Andes 3200 masl site, Peters et al. (2013) installed a soil monitoring station that recorded soil temperature and soil moisture data from February 2010 to January 2011. 50 cm MSST and WMMST at the site were 13 and 16.9 °C, respectively. Mean summer soil moisture at 50 cm depth was 0.09 $m^3 m^{-3}$ over the same period. Oxygen isotope measurements at the sample site are limited. Peters et al. (2013) collected precipitation samples from the site sporadically between October 2008 and October 2010, but due to the limited sample set, the standard deviation for these measurements is large (±7‰). Hoke et al. (2009) collected additional precipitation samples in the same valley, as well as river water samples from the nearby Río Mendoza (elevations range from 3000 to 3300 masl). Based on the observed $\delta^{18}O$ values of this suite of samples, the range in soil water $\delta^{18}O$ at the 3200 masl site is assumed to be −17 to −9‰.

4.1.3. Tibet, China

The temperature and precipitation data for the Lhasa, Shigatse, and T'u-ko-erh-ho-kung, Tibet weather stations are summarized in Table 3. All three sites are influenced by the Indian monsoon and have a summer wet season, with Lhasa, Shigatse, and T'u-ko-erh-ho-kung receiving 63%, 71%, and 57%, respectively, of their annual rainfall between June and August. GNIP data show that between 1986 and 1992 the mean $\delta^{18}O$ of rainwater at Lhasa was −13‰ VSMOW, which compares favorably to nearby river and meteoric water samples collected by Quade et al. (2011), which have $\delta^{18}O$ values between −16 and −13‰. $\delta^{18}O$ values from stream and meteoric waters collected near the Shigatze and T'u-ko-erh-ho-kung soils range from −19 to −15‰ (Table 2, Quade et al., 2011).

4.1.4. Svalbard, Norway, the High Arctic

The Ny-Ålesund, Svalbard weather station (which is located roughly 10 km from the Cannes and Kapp Guissez sample sites) records a MST of 7 °C for the period 1998 to 2014, (Fig. 1B). WMMT was 9 °C for the same period. Modern 50 cm MSST from a permafrost borehole near Ny-Ålesund is 3 °C, and WMMST at the same depth is 5 °C (Paulik et al., 2014), consistent with August soil temperatures between 0.5 and 10 °C measured at the Cannes site Mann et al. (1986). Soil moisture data were unavailable for the Svalbard study sites, but 1998–2014 weather station data show that there is strong autumn-winter bias in precipitation, with an average of 245 mm of precipitation falling between September and February, and an average of 140 mm falling between March and August. Courty et al. (1994) reported local snow $\delta^{18}O$ values of −8 to −6‰ for the Cannes site discussed in this study; however, this was a single measurement and probably does not capture local variability in precipitation $\delta^{18}O$. Additional long-term meteoric water $\delta^{18}O$ values were recorded at the Ny-Ålesund GNIP station from 1990 to 2015, and have a mean value of −11.6‰ with a standard deviation of 2.8‰. In order to make a conservative estimate of the carbonate $\delta^{18}O$ anomalies for the High Arctic samples, we used the longer term (15 years) GNIP mean $\delta^{18}O$ value of

−11.6‰, and assumed that the range in local meteoric water $\delta^{18}O$ values was −14 to −8‰ (range encompasses the mean GNIP $\delta^{18}O$ value ± the standard deviation [2.8‰]).

4.2. X-ray diffraction results

X-ray diffraction analysis was performed on the Kapp Guissez (KG-201a, KG-201b) and Cannes (Cannes-30) High Arctic samples to assess the impact of the presence of dolomitic parent material in the soil profiles. X-ray diffraction analysis was not performed on the other samples either because there was no dolomitic parent material in the sampled soils, or (in the case of the sub-glacial carbonates) because previous studies had shown that the carbonate precipitates had little to no dolomitic inclusions (Hanshaw and Hallet, 1978). X-ray diffraction results show that the Cannes-30 sample is composed of 20% dolomite and 80% calcite. Mann et al. (1986) noted the presence of detrital dolomitic silt in the Cannes soil, suggesting that the dolomite in the Cannes-30 sample is likely detrital in origin. This sample was not analyzed further. In contrast, x-ray diffraction analysis showed that the Cannes-62 sample is composed of 70% aragonite and 30% calcite, with no measurable dolomite fraction. Because past studies (Schauble et al., 2006; Eagle et al., 2013; Henkes et al., 2013; Wacker et al., 2013) have shown that clumped isotope results for calcite and aragonite are indistinguishable under current analytic uncertainties, we proceeded with clumped isotope analysis for the Cannes-62 sample.

4.3. Δ_{47}, $\delta^{18}O$, and $\delta^{13}C$ results

Soil carbonate and sub-glacial $\delta^{18}O$, $\delta^{13}C$, and Δ_{47} values are reported in Table 4 and in Table SI2 in the Supplementary Information, along with calculated apparent T (Δ_{47}) values. The $\delta^{18}O$ values of the Cannes-62 sample were adjusted to account for the difference in $\delta^{18}O$ CO_2-carbonate fractionation factors (Kim et al., 2007) between calcite and aragonite (see Supplementary Information). $\delta^{18}O$ (VPDB) values range from −3.1 to −20.3‰ for the soil carbonate samples, and −18.3 to −10.2‰ for the sub-glacial carbonate samples. The mean external error (1 standard error) for all carbonate $\delta^{18}O$ measurements is ±0.09‰. $\delta^{13}C$ values range between −5.4 and 10.4‰ for the soil carbonates and −1.1 and 2.4‰ for the sub-glacial carbonates, and yield a standard error of ±0.05‰. Observed sample average Δ_{47} values range from 0.618 to 0.680‰ for the soil carbonate samples analyzed in the UW Isolab, 0.683 to 0.708‰ for the Peters et al. (2013) samples (analyzed at Caltech), and 0.410–0.684‰ for the sub-glacial carbonates. The mean standard error for all Δ_{47} measurements is ±0.012‰.

For all samples except the Argentinian Andes soil carbonates, T(Δ_{47}) values were calculated from the Δ_{47} results using the Δ_{47}-T calibration of Kelson et al. (2017) (Eq. (1); 90 °C acid reaction, no acid correction). For the Argentinian Andes samples, see Peters et al. (2013) for complete methods description. Apparent T(Δ_{47}) values for the sub-glacial carbonates are highly variable, ranging from 96 to

Table 4
Clumped and stable isotope data for all soil and sub-glacial carbonates.

Sample name	n	$\delta^{13}C_{carb}$ (‰) VPDB	±1 SE (‰)	$\delta^{18}O_{carb}$ (‰) VPDB	±1 SE (‰)	Mean $\delta^{18}O$ Anomaly (‰)						Δ_{47} (‰) ARF	±1 SE (‰)	Mean Δ_{47} Anomaly (‰)			$T(\Delta_{47})$ (°C)	±1 SE (°C)
						−1 °C CFT[a]		MST CFT		WMMT CFT				−1 °C CFT	MST CFT	WMMT CFT		
						Low $\delta^{18}O$[b]	High $\delta^{18}O$	Low $\delta^{18}O$	High $\delta^{18}O$	Low $\delta^{18}O$	High $\delta^{18}O$							
Elq13-4700-20	3	9.43	0.06	−3.10	0.06	11.99	6.96	14.26	9.25	14.48	9.47	0.6391	0.0093	−0.063	−0.024	−0.020	16	3
Elq13-4700-40	4	8.52	0.03	−3.82	0.08	11.26	6.24	13.09	8.08	13.54	8.52	0.6245	0.0111	−0.077	−0.046	−0.038	20	3
Elq13-4700-60	4	10.00	0.02	−4.17	0.05	10.92	5.89	12.75	7.73	13.19	8.18	0.6321	0.0080	−0.070	−0.038	−0.031	18	2
Elq13-4700-80	3	10.36	0.04	−5.17	0.05	9.92	4.89	11.75	6.73	12.19	7.18	0.6462	0.0093	−0.056	−0.024	−0.017	14	3
Elq13-4700-100	5	9.25	0.04	−6.35	0.07	8.73	3.71	10.57	5.55	11.01	5.99	0.6323	0.0072	−0.070	−0.038	−0.031	18	2
Elq13-4500-50	7	9.14	0.05	−9.16	0.03	5.93	0.90	8.20	3.19	8.64	3.63	0.6803	0.0109	−0.022	0.018	0.025	5	3
Elq13-4200-50	5	6.88	0.04	−4.56	0.06	7.51	5.50	10.22	8.22	10.65	8.65	0.6581	0.0080	−0.044	0.003	0.010	10	2
Elq13-3750-50	6	0.87	0.03	−11.59	0.11	−0.52	−2.53	2.84	0.84	3.26	1.26	0.6671	0.0072	−0.035	0.022	0.029	8	2
Elq13-3550-20	5	2.92	0.14	−5.79	0.18	4.27	1.26	8.06	5.06	8.06	5.06	0.6463	0.0105	−0.056	0.009	0.009	14	3
Peters-B15	4	−2.08	0.04	−10.66	0.04	1.41	−6.63	4.98	−3.03	5.40	−2.61	0.6835	0.0139	−0.096	−0.010	0.000	17	3
Peters-B30	2	−5.37	0.04	−11.83	0.05	0.24	−7.80	3.60	−4.41	4.23	−3.78	0.6831	0.0215	−0.096	−0.015	0.000	17	4
Peters-B45	4	−4.67	0.04	−12.84	0.02	−0.77	−8.81	2.59	−5.42	3.01	−5.00	0.7076	0.0080	−0.072	0.010	0.019	12	2
ANT-1	3	6.86	0.10	−14.41	0.15	13.75	9.73	13.75	9.73	14.44	10.42	0.6383	0.0093	−0.064	−0.064	−0.052	16	3
ANT-2	3	8.36	0.08	−17.81	0.14	10.34	6.32	10.57	6.55	11.26	7.24	0.6323	0.0093	−0.070	−0.066	−0.054	18	3
ANT-3	3	8.90	0.09	−17.87	0.20	10.28	6.26	10.51	6.49	11.20	7.18	0.6493	0.0093	−0.053	−0.049	−0.037	13	3
ANT-4	3	9.32	0.04	−20.34	0.17	7.81	3.79	8.04	4.02	8.73	4.71	0.6487	0.0093	−0.053	−0.049	−0.037	13	3
KG-201a	3	−0.42	0.01	−7.51	0.10	1.54	−4.49	2.48	−3.54	2.94	−3.08	0.6485	0.0093	−0.054	−0.037	−0.029	13	3
KG-201b	3	0.53	0.02	−7.11	0.17	1.94	−4.09	2.88	−3.14	3.34	−2.68	0.6305	0.0093	−0.071	−0.055	−0.047	18	3
Cannes-62	3	5.31	0.07	−5.03	0.06	4.03	−2.01	4.96	−1.06	5.42	−0.60	0.6779	0.0093	−0.024	−0.008	0.000	5	2
Tsangpo-19a	3	3.30	0.05	−14.71	0.10	−2.64	−4.65	0.72	−1.29	0.93	−1.07	0.6573	0.0093	−0.045	0.013	0.016	11	3
Tsangpo-19b	3	3.79	0.08	−14.21	0.04	−2.13	−4.14	1.23	−0.78	1.44	−0.57	0.6648	0.0093	−0.037	0.020	0.024	8	2
Tsangpo-21a	3	−2.91	0.03	−11.65	0.04	2.43	−0.59	5.99	2.99	5.99	2.99	0.6600	0.0093	−0.042	0.019	0.019	10	3
Tsangpo-21b	3	−2.94	0.05	−13.59	0.04	0.50	−2.52	4.06	1.06	4.06	1.06	0.6248	0.0133	−0.077	−0.016	−0.016	20	4
Tsangpo-22	4	−1.45	0.04	−15.74	0.06	−2.67	−3.67	0.90	−0.10	0.90	−0.10	0.6184	0.0080	−0.084	−0.023	−0.023	22	3
Lhasa-4	3	−3.98	0.05	−17.33	0.09	−8.28	−10.29	−4.49	−6.49	−4.28	−6.28	0.6355	0.0094	−0.067	−0.002	0.001	17	3
CG-1	3	0.53	0.09	−10.23	0.17	4.86	3.85	NA	NA	5.09	4.09	0.4451	0.0093	−0.257	−0.253	−0.253	96	6
CG-2	3	2.42	0.01	−11.16	0.02	3.93	2.92	NA	NA	4.16	3.16	0.4102	0.0112	−0.292	−0.288	−0.288	119	8
BF-1	3	−1.14	0.02	−18.26	0.03	−8.20	−9.20	NA	NA	−7.96	−8.97	0.6839	0.0108	−0.018	−0.014	−0.014	4	3
BF-2	4	−0.77	0.01	−17.06	0.09	−7.00	−8.01	NA	NA	−6.76	−7.77	0.5969	0.0104	−0.105	−0.101	−0.101	29	4
BF-3	3	−0.87	0.04	−16.61	0.11	−6.55	−7.56	NA	NA	−6.31	−7.32	0.5790	0.0093	−0.123	−0.119	−0.119	35	3

[a] FT = carbonate formation temperature; see Table 2 for the MST and WMMT estimates for each site.
[b] See Table 2 for the high and low $\delta^{18}O$ estimates for each site.

119 °C for the Castleguard Glacier samples (2 samples, 3 replicates each), to 4–35 °C for the Blackfoot Glacier samples (3 samples, 3 to 4 replicates each). The mean standard error in T(Δ_{47}) estimates for the sub-glacial carbonates is ±5 °C. In contrast to the sub-glacial samples, the soil carbonates show a much smaller degree of variability in T (Δ_{47}) values. Apparent formation temperatures for individual samples range from 5 °C (Cannes-62) to 22 °C (Tsangpo-22), within the range of Earth-surface temperatures. The standard error in T(Δ_{47}) for the soil carbonate samples is ±3 °C. Mean T(Δ_{47}) is 15 °C for the Antarctica samples, 17 and 14 °C for the 4700 and 3550 masl Chilean Andes samples, 12 °C for the Arctic carbonates, and 16 °C for the Tibetan samples. Supplementary Fig. 1 shows soil carbonate T(Δ_{47}), mean monthly air temperature and (where available) mean monthly soil temperature, mean monthly precipitation, and mean monthly soil moisture for the soil sample sites in the Andes, Antarctica, the High Arctic, and Tibet.

The Tibetan Plateau samples analyzed for this study are distinct nodules collected from the same sites and soil horizons as the samples reported in Quade et al. (2013). The $\delta^{18}O$, $\delta^{13}C$, and Δ_{47} values for our new nodules are generally consistent with the Quade et al. (2013) samples, though they do display some heterogeneity. For all of the soil sites, the difference in measured $\delta^{13}C$ values is within 2‰, which

is similar to the variability observed between the original Quade et al. (2013) samples (Table SI3). With respect to $\delta^{18}O$ and Δ_{47}, the differences for the Tsangpo-19, Tsangpo-22, and Lhasa-4 samples are less than 3‰ or 2 °C respectively; but the Tsangpo-21 site yields much larger differences (6‰ and 8 °C respectively). The differences between the samples analyzed for this study and those analyzed previously by Quade et al. (2013) appear to be due to natural variability in the isotopic composition of the carbonate pendants within any given horizon.

4.4. Δ_{47}, $\delta^{18}O$, and $\delta^{13}C$ anomalies

The calculated −1 °C, MST/MSST, and WMMT/WMMST Δ_{47} anomalies for our soil carbonate samples exhibit a 0.1‰ range of values (Fig. 4), with some samples yielding values near the 0‰ expected for equilibrium carbonates, and other samples being significantly more negative suggesting disequilibrium processes. Some uncertainty in calculated anomalies is introduced depending on the assumed local carbonate formation temperature at each site (Table 4). For the colder Arctic and Antarctic sites, the difference between the minimum assumed carbonate formation temperature of −1 °C and the local MSST and WMMST is relatively small, leading to small uncertainty in calculated Δ_{47} anomalies that are on the order of typical
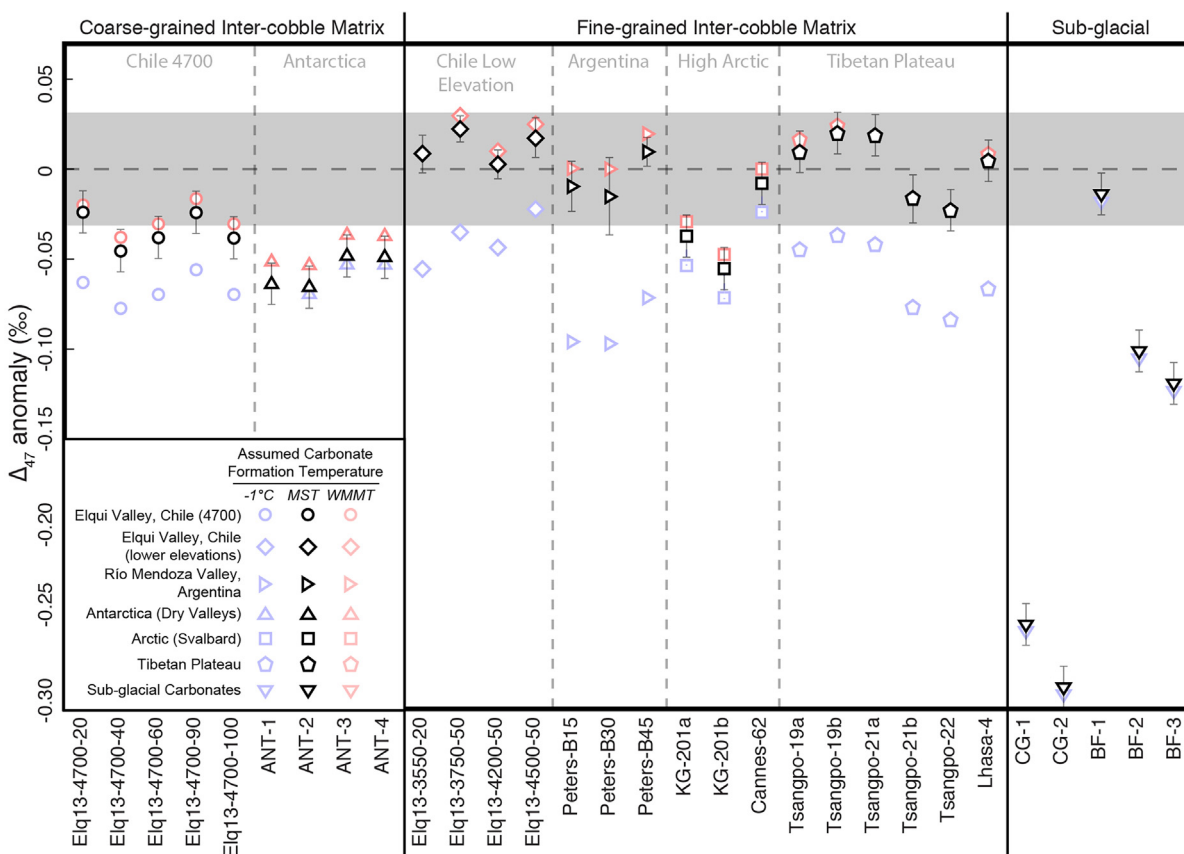

Fig. 4. Calculated carbonate Δ_{47} anomalies arranged by soil matrix type. The dashed horizontal line marks a Δ_{47} anomaly of 0‰, and the dark gray band shows the 95% confidence interval (external error) around that line.

analytical uncertainty in Δ_{47}. The Chilean soil carbonates exhibit larger variations in Δ_{47} anomaly calculated using different assumed formation temperatures, reflecting the greater difference between $-1\,°C$ and the warmer local MSST and WMMST.

For those samples from soils with coarse grained inter-cobble matrices (n = 9; the Antarctic and 4700 masl Chilean samples), all of the calculated Δ_{47} anomalies are negative regardless of whether the soil carbonates are assumed to have formed at $-1\,°C$, local MAT or MSST, or local WMMST (Fig. 4). The mean Δ_{47} anomaly for the Antarctic soil carbonates is $-0.060‰$ at $-1\,°C$, $-0.057‰$ at local MSST, and $-0.045‰$ at local WMMST, and the 4700 masl Chilean soil carbonate samples have a mean Δ_{47} anomaly of $-0.067‰$ at $-1\,°C$, $-0.034‰$ at local MST, and $-0.027‰$ at local WMMT. If the Chilean and Antarctic Δ_{47} anomalies are calculated using an assumed carbonate formation temperature of $-1\,°C$, the resulting values are all significantly below 0‰ (e.g., they fall outside the 95% confidence interval (CI) for the expected Δ_{47} value for equilibrium carbonates). When MSST or WMMST are used to calculate the Δ_{47} anomalies, all of the Antarctic samples and one of the Chilean samples (Elq13-4700-40) are still significantly below 0‰.

In contrast, the sample from soils that have relatively fine grained inter-cobble matrices (n = 16; the 3550, 3750, 4200, and 4500 masl Chilean, Argentina, Svalbard, and Tibet samples) yield Δ_{47} anomalies calculated using mean summer air or soil temperatures and warmest mean monthly air or soil temperatures that are indistinguishable from 0‰ (i.e., they fall within the 95% CI of the expected equilibrium carbonate Δ_{47} composition; Fig. 4). The exception to this trend are the samples from Kapp Guissez, Svalbard: the KG-201b sample has a significant negative Δ_{47} anomaly, and the Δ_{47} anomaly for sample KG-201a from the same locality falls slightly outside the 95% confidence interval when calculated using MST. When the fine-matrix samples (n = 16) Δ_{47} anomalies are calculated using a formation temperature of $-1\,°C$, every sample except Cannes-62 falls outside the 95% CI for the Δ_{47} value of expected equilibrium carbonates Fig. 4).

The sub-glacial carbonate Δ_{47} anomalies yield a much wider range in values than observed in the soil carbonates, and only one of the sub-glacial samples has a Δ_{47} anomaly that falls within the 95% CI for the Δ_{47} value of expected equilibrium carbonates (Fig. 4). Sample BF-1 from Blackfoot Glacier falls within the 95% CI for the Δ_{47} value of expected equilibrium carbonates, while the Δ_{47} anomalies for the other two Blackfoot sub-glacial samples are much larger and negative (-0.105 to $-0.123‰$); as a result, individual samples from this site display a much wider range in Δ_{47} anomaly values than any of our other sample sites. The Δ_{47} anomalies for the Castleguard sub-glacial samples are -0.257 to $-0.292‰$ at $-1\,°C$, which is an order of magnitude more negative than any of the soil carbonate samples.

The soil carbonate $\delta^{18}O$ anomalies for the samples with relatively coarse grained inter-cobble matrices (i.e., 4700 masl Chilean Andes and Antarctic samples) are one to
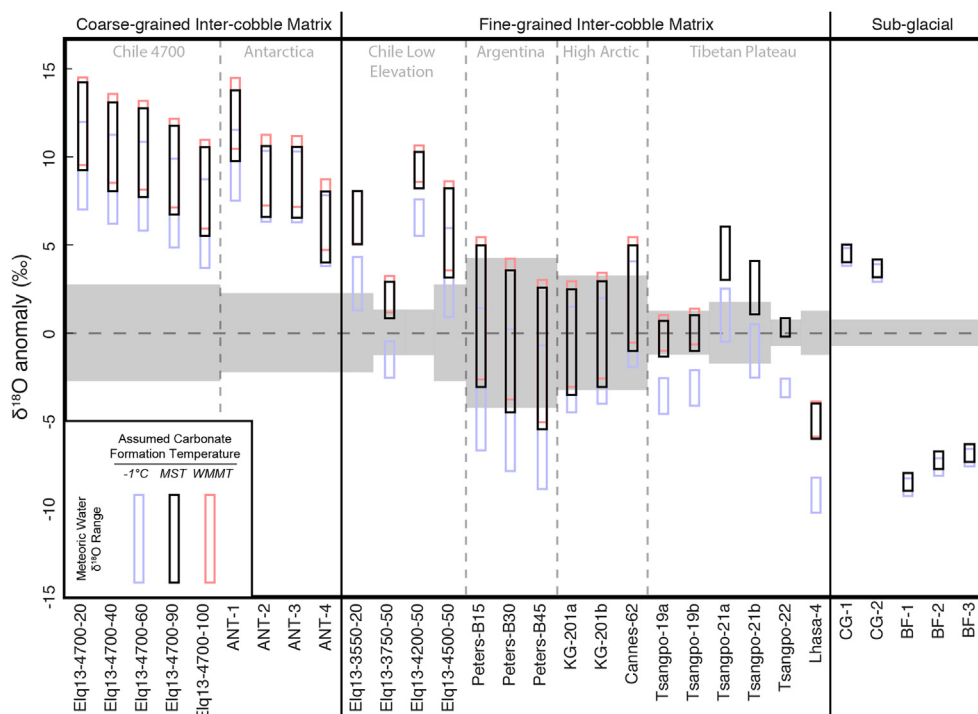

Fig. 5. Calculated carbonate $\delta^{18}O$ anomalies arranged by soil matrix type. Black bars represent the range in $\delta^{18}O$ anomalies calculated for local mean summer air or soil temperature and the range of local meteoric water $\delta^{18}O$ values. Red bars represent the range in $\delta^{18}O$ anomalies calculated for local warmest mean monthly air or soil temperature. Blue bars represent the range in $\delta^{18}O$ anomalies calculated for $-1\,°C$. The dashed horizontal line marks a $\delta^{18}O$ anomaly of 0‰, and the gray band shows the uncertainty around that line (calculated for each sample as the difference between the maximum and minimum local meteoric $\delta^{18}O$ values plus the analytical error [1 SE]).

two orders of magnitude larger than the calculated Δ_{47} anomalies, but display a similar pattern in that they are consistently different from the expected equilibrium value regardless of assumed formation temperature. The $\delta^{18}O$ anomalies for the coarse-grained matrix samples are all large and positive (>3‰), and very high relative to all of the other soil and sub-glacial carbonate samples, except the lower elevation Chilean samples which are comparable (Fig. 5). The range in Δ_{47} anomalies for the Antarctic and 4700 masl Chilean samples is too small (<0.025‰) to determine if there is a significant Δ_{47}- $\delta^{18}O$ correlation; however, these samples plot near the lower limit of the 0.005 ± 0.003‰ slope observed by Kluge et al. (2014) in coarse-grained cryogenic cave carbonates, and significantly above the 0.02‰ slope predicted by Guo (2009) (Supplementary Fig. 2).

The $\delta^{18}O$ anomalies for the samples with relatively fine-grained inter-cobble matrices (i.e., 3550, 3750, 4200 and 4500 masl Chilean Andes, Argentinian Andes, High Arctic, and Tibet samples) yield mixed results. With values of 2.8‰ at −1 °C, 5.8‰ at MSST, and 6.2‰ at WMMST, the mean $\delta^{18}O$ anomaly for the lower elevation Chilean samples (3550, 3750, 4200, and 4500 masl) is positive and large, similar to the smallest anomalies from the coarse-grained matrix sample suite. The Argentinian Andes samples (n = 3) have relatively large ranges in possible $\delta^{18}O$ anomalies due to the large range in observed meteoric water $\delta^{18}O$ values at the 3200 masl sample site. Despite this large range, the Argentinian Andes anomalies cluster about the 0‰ line. The High Arctic sample $\delta^{18}O$ anomalies (n = 3) yield either negative or positive results depending on whether the $\delta^{18}O$ anomalies are calculated using the maximum or minimum local meteoric water $\delta^{18}O$ values, respectively. The Tibetan plateau sample $\delta^{18}O$ anomalies (n = 6) are small and scattered about 0‰.

The sub-glacial $\delta^{18}O$ anomalies yield different results, with the Castleguard glacier samples having large positive $\delta^{18}O$ anomalies, and the Blackfoot glacier samples yielding large negative $\delta^{18}O$ anomalies.

To test the dependence of our $\delta^{18}O$ anomalies on the choice of calcite-water $\delta^{18}O$ calibration, we recalculated the anomalies using the calibration of Kim and O'Neil (1997). For all of our samples, the Kim and O'Neil (1997) $\delta^{18}O$ anomalies are ~1.61‰ larger than the Watkins et al. (2014) $\delta^{18}O$ anomalies (Supplementary Fig. 3). This difference is expected, since the Kim and O'Neil (1997) calibration is isotopically light relative to the Watkins et al. (2014) calibration. The difference between the Kim and O'Neil (1997) and Watkins et al. (2014) $\delta^{18}O$ anomalies does not change our interpretations of the data, and for the remainder of this paper only the Watkins et al. (2014) $\delta^{18}O$ anomalies will be discussed.

The lack of soil CO_2 stable isotope data limits our ability to calculate precise $\delta^{13}C$ anomalies for most soil carbonate samples, but we can nevertheless compare the observed sample $\delta^{13}C$ values to the expected range of equilibrium soil carbonate $\delta^{13}C$ values. Fig. 6 shows the expected $\delta^{13}C$ values for soil carbonates precipitated in isotopic equilibrium with two separate CO_2 reservoirs: atmospheric CO_2 (lower gray band), and CO_2 respired by C3 plants (upper gray
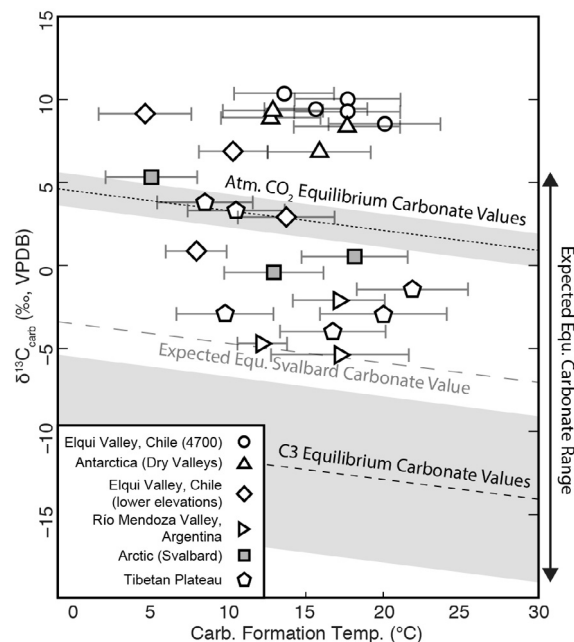

Fig. 6. Carbonate $\delta^{13}C$ values plotted against carbonate formation temperature (°C). The dark dotted and dashed lines represent the mean $\delta^{13}C$ values of carbonates forming in equilibrium with atmospheric and C3 plant-respired CO_2 (Cerling and Quade, 1993), respectively, with the gray bands showing the uncertainty associated with these values. The dashed light gray line shows the soil CO_2 $\delta^{13}C$ values measured at the Cannes, Svalbard soil site by Marlin et al. (1993). The sample symbols are the same as in Fig. 5, save that the Svalbard High Arctic samples are highlighted as dark gray squares. The dark symbols plot the sample $T(\Delta_{47})$ versus sample $\delta^{13}C$, with the associated 1 SE error bars. Note that equilibrium soil carbonates would be expected to plot between the atmospheric and C3 equilibrium carbonates values (see range marked by arrows to the right of the graph).

band) (Cerling and Quade, 1993; Kohn, 2010). As shown in Fig. 6, the coarse-grained inter-cobble matrix (i.e., Antarctic and 4700 masl Chilean Andes) carbonates plot at or above the upper limit of expected values for soil carbonates that have formed in isotopic equilibrium with atmospheric CO_2 (pre-industrial = −6.5‰; modern = −8.5‰), regardless of the assumed carbonate formation temperature. The $\delta^{13}C$ values of most of the fine-matrix samples (i.e., two of the lower elevation Chilean samples, and the Argentinian and Tibetan Plateau samples) generally fall within the range of equilibrium carbonates forming from atmospheric and plant-respired CO_2. In contrast, the carbonate $\delta^{13}C$ values of two of the lower elevation Chilean samples (4200 and 4500 masl samples) are higher than the upper limit of expected equilibrium carbonate $\delta^{13}C$ values. Similarly, the $\delta^{13}C$ values for the High Arctic samples (KG-201a, KG-201b, and Cannes-62) are higher than soil CO_2 $\delta^{13}C$ values measured by Courty et al. (1994) at the Cannes soil site.

5. DISCUSSION

The calculated Δ_{47}, $\delta^{18}O$, and $\delta^{13}C$ anomalies enable us to assess equilibrium versus KIE processes in carbonate

proxy archives from cold environments. We find that the Δ_{47}, $\delta^{18}O$, and $\delta^{13}C$ anomalies of the lower elevation Chilean Andes, Argentinian Andes, and Tibetan and High Arctic soil carbonates (collected from soils with a silt to sand matrix component) are consistent with summer formation of soil carbonate under conditions near isotopic equilibrium; however the isotopic composition of the lower elevation Chilean and High Arctic soil carbonates appear to have been affected by extreme aridity and dissolution/reprecipitation, respectively. In contrast, the Δ_{47}, $\delta^{18}O$, and $\delta^{13}C$ anomalies of the Antarctic and 4700 masl Chilean Andes soil carbonates (collected from soils that lack a silt or finer sand component in the soil matrix) are consistent with cryogenic carbonate formation and KIE due to rapid CO_2 degassing during bicarbonate dehydration. The sub-glacial carbonates from both glacier sites yield negative Δ_{47} anomalies, but distinctly different $\delta^{18}O$ anomalies that may be consistent with differences in sub-glacial plumbing and resulting variations in meltwater salinity and pH. We attribute the observed site-to-site variability in soil carbonate Δ_{47}, $\delta^{18}O$, and $\delta^{13}C$ anomalies to differences in inter-cobble soil matrix grain size and attendant differences in soil moisture, and discuss the implications of our findings with respect to past and future paleoclimate studies based on soil carbonates from cold climates.

5.1. Isotopic equilibrium and disequilibrium in cold-climate soil carbonates

5.1.1. equilibrium soil carbonates from fine-matrix soils from the Tibetan Plateau, High Arctic, and the Chilean and Argentinian Andes

First we examine the isotopic results from soils with fine-grained inter-cobbles matrices, i.e., those samples collected from the 3550, 3750, 4200, and 4500 masl sites in the Chilean Andes, as well as the Argentinian Andes, Tibetan Plateau, and High Arctic sites. Due to the reduced pore space and permeability (e.g., hydraulic conductivity) in these soils, we expect them to experience slower rates of CO_2 degassing, which in turn should favor equilibrium soil carbonate formation. Equilibrium soil carbonates are predicted to have $T(\Delta_{47})$ values in the range of local soil temperatures: similar to local MAT, or local winter or summer soil temperatures if there is a seasonal bias to soil carbonate formation (Peters et al., 2013; Quade et al., 2013; Hough et al., 2014; Burgener et al., 2016; Gallagher and Sheldon, 2016; Ringham et al., 2016). Equilibrium soil carbonate $\delta^{18}O$ values should be consistent with the isotopic composition of local meteoric waters (after taking into account the temperature-dependent calcite-water fractionation factor), but may be more positive by $\leq 10‰$ due to evaporative effects (Liu et al., 1996; Quade et al., 2007; Burgener et al., 2016). Equilibrium soil carbonate $\delta^{13}C$ should fall between the $\delta^{13}C$ values of atmospheric CO_2 and C3 plant-respired CO_2 (after taking into account the temperature dependent ^{13}C fractionation between CO_2 and calcite; see Fig. 6).

The Peters et al. (2013) Argentinian Andes samples all yield negligible Δ_{47} and $\delta^{18}O$ anomalies and $\delta^{13}C$ values that are consistent with equilibrium carbonate formation.

Sample Δ_{47} values are consistent with measured local mean summer soil temperatures. The samples show a large range in $\delta^{18}O$ anomalies that are consistent with the range of meteoric water $\delta^{18}O$ values observed in this study area. It is interesting to note that the values of these anomalies decrease with depth, which is characteristic of soil profiles that have experienced enrichment of soil water $\delta^{18}O$ nearer the soil surface due to the effects of evaporation (Liu et al., 1996). We attribute the large ranges in the $\delta^{18}O$ anomalies of these samples to uncertainties in the long-term range of meteoric water $\delta^{18}O$ values. Because the $\delta^{18}O$ anomalies all center on the 0‰ line (Fig. 5), we interpret them as being consistent with equilibrium carbonate formation. The soil carbonate $\delta^{13}C$ values plot well within the range of expected soil $CO2$ $\delta^{13}C$ values.

In regard to the Tibetan Plateau samples, Quade et al. (2011) showed that most of the soil carbonates they analyzed from the Tibetan plateau exhibit a summer-season bias in their $\delta^{18}O$ values; therefore we expected that the Δ_{47} and $\delta^{18}O$ anomalies calculated using local MST and WMMT would be small, consistent with equilibrium, seasonally biased carbonate formation. The $T(\Delta_{47})$ values of these samples are in line with local summer soil temperatures (Supplementary Fig. 1E, F, and G), and their average Δ_{47} anomalies calculated using MST/WMMT are smaller than our analytical uncertainties (0.002‰ and 0.003‰, respectively). Additionally, their $\delta^{13}C$ values fall between the ranges of expected $\delta^{13}C$ values for soil carbonates that formed in equilibrium with some mixture of atmospheric and soil CO_2 (Fig. 6), consistent with this hypothesis.

We suggest that the differences from 0‰ (e.g., apparent equilibrium) observed for some of the Tibetan Δ_{47} and $\delta^{18}O$ anomalies (e.g., the Lhasa-4 $\delta^{18}O$ anomaly) calculated for local MST and WMMT (Figs. 5 and 7) can be explained by three factors, with no need to invoke disequilibrium processes. First, variable conditions in local soil and climate, as well as small differences in mean soil carbonate age, mean that our samples may include carbonate that precipitated at different times in the past and under slightly different temperature and meteoric water $\delta^{18}O$ conditions. Second, due to the lack of long-term soil temperature measurements, we were forced to estimate mean soil temperature conditions at the sampling sites using data from meteorological stations that are located up to 130 km away (see Table 3), introducing unquantified uncertainties into our soil temperature estimates and the subsequent anomaly calculations. Third, our calculations of equilibrium carbonate $\delta^{18}O$ values also contain uncertainties due to (1) the distance between the sample soil sites and GNIP stations or individual water samples collected by Quade et al. (2011); (2) the short temporal coverage and data gaps in the available GNIP records; and (3) the fact that our calculations are based on meteoric and stream water $\delta^{18}O$ values that do not take into account evaporative effects that commonly enrich soil waters relative to local meteoric waters (Liu et al., 1996; Quade et al., 2007; Burgener et al., 2016).

After taking into account variations due to uncertainties in local temperature and meteoric water $\delta^{18}O$ values, we interpret the Δ_{47}, $\delta^{18}O$, and $\delta^{13}C$ results of the Tibetan
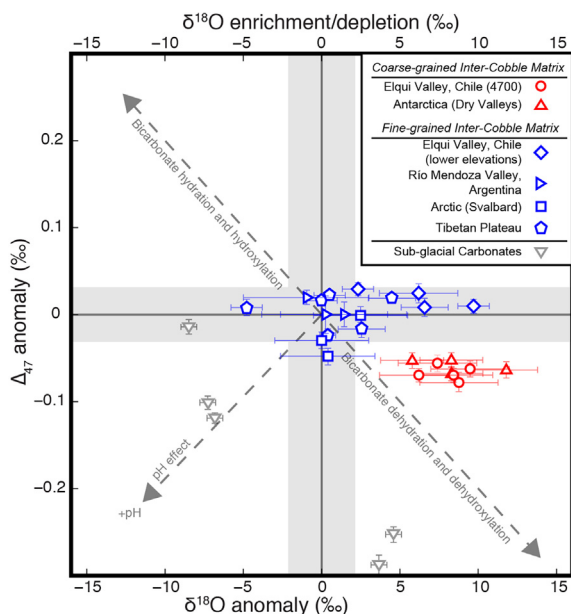
Fig. 7. Estimated Δ_{47} and $\delta^{18}O$ anomalies for the coarse-grained inter-cobble matrix soils (red symbols), fine-grained inter-cobble matrix soils (blue symbols), and sub-glacial samples (gray symbols). All samples are plotted using the favored precipitation temperature as discussed in Section 5 of this study (e.g., −1 °C for the coarse-grained inter-cobble matrix samples, and local WMMT/WMMST for the fine-grained inter-cobble matrix samples). Horizontal error bars show the range in $\delta^{18}O$ anomalies based on local meteoric water $\delta^{18}O$ values. Vertical error bars show the range in Δ_{47} anomalies based on local air or soil temperature uncertainties. The dark gray dashed lines show the disequilibrium tendencies of various disequilibrium carbonate precipitation processes, as in Fig. 2. Schematic modified from Tripati et al. (2015). The vertical gray band shows the 95% confidence interval about the 0‰ line for the Δ_{47} anomalies; the horizontal gray band shows the uncertainty around the 0‰ line for the $\delta^{18}O$ anomalies (calculated for each sample as the difference between the maximum and minimum local meteoric $\delta^{18}O$ values plus the analytical error [1 SE]). (For interpretation of the references to colour in this figure legend, the reader is referred to the web version of this article.)

Plateau soil carbonate samples as being consistent with calcite formation under conditions of apparent isotopic equilibrium. This interpretation is supported by the fact that no single process (e.g., bicarbonate dehydration or the pH effect) can account for the Δ_{47} and $\delta^{18}O$ anomalies observed in these samples. For example, KIEs associated with bicarbonate dehydration during cryogenic carbonate formation should result in enrichment in soil carbonate ^{18}O relative to the expected equilibrium carbonate composition (e.g. a positive $\delta^{18}O$ anomaly), and depletion in soil carbonate Δ_{47} relative to the expected equilibrium clumped isotope composition (e.g. a negative Δ_{47} anomaly) for all samples. This is not observed in our Tibetan samples, which instead have Δ_{47} anomalies indistinguishable from expected equilibrium values, and variable (positive and negative) $\delta^{18}O$ anomalies. Alternatively, as shown in Fig. 8, if we assume a normal range in soil pH (7–8.5; Brady and Weil, 2010) for the Tibet soils, their carbonate $\delta^{18}O$ values do not appear to be in good agreement with $\delta^{18}O$ values for
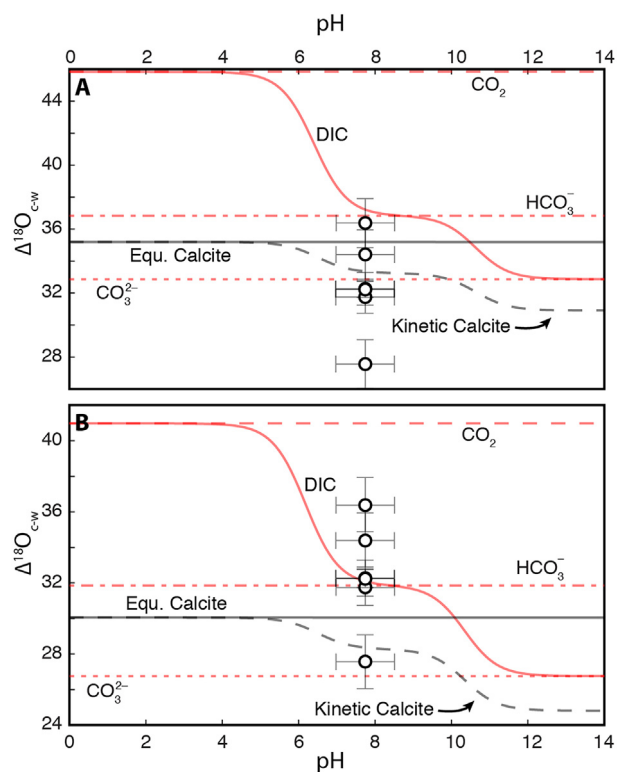

Fig. 8. Modeled pH-dependence of disequilibrium calcite $\delta^{18}O$ values at 0 °C (A), and mean Lhasa/Shigatse summer temperatures (23.5 °C; B). Circles show the calculated $\delta^{18}O$ disequilibrium values for the Tibet soil carbonates. Soil pH values were estimated using mean global soil pH values (Brady and Weil, 2010).

carbonates that have experienced the disequilibrium "pH effect", as predicted using the process-based model developed by Watkins and Hunt (2015), which calculates Δ_{47}, $\delta^{18}O$, $\delta^{13}C$ values for non-equilibrium carbonates. Based on these observations, we deem it most reasonable to attribute the relationship between the observed carbonate isotope values ($T(\Delta_{47})$, $\delta^{18}O$, and $\delta^{13}C$) and local environmental conditions to equilibrium carbonate formation processes rather than to some combination of disequilibrium processes.

We also interpret the lower elevation Chilean Andes (i.e., 3550, 3750, 4200, and 4500 masl) Δ_{47} and $\delta^{18}O$ anomalies, and $\delta^{13}C$ values as being consistent with equilibrium carbonate formation in arid conditions, after taking into account the effects of evaporation on soil carbonate $\delta^{18}O$ values. The Δ_{47} anomalies for these four samples are indistinguishable from 0‰ at the 95% CI. The positive 5–8‰ $\delta^{18}O$ anomaly observed for this site can be explained by the large degree of evaporation observed in arid soils (Quade et al., 2007). Our calculation of the $\delta^{18}O$ anomaly was based on the maximum and minimum observed $\delta^{18}O$ composition of local meteoric waters, which do not experience as much evaporation and ^{18}O-enrichment as local soil water. Any soil carbonates that precipitate from soil water solutions that are evaporatively enriched in ^{18}O will inherit the heavy ^{18}O composition of the soil water, and should have a positive $\delta^{18}O$ anomaly relative to local meteoric waters. Quade et al. (2007) found that soil water in the

Atacama desert is evaporatively enriched relative to local meteoric waters by up to ~10‰. Because the low elevation Chilean study area is less arid than the Atacama Desert, we suggest that soil waters at these sites could have experienced ~6‰ evaporative enrichment. After taking this evaporative enrichment into account, we interpret the $\delta^{18}O$ value of these samples as being consistent with the expected equilibrium carbonate composition.

With respect to carbonate $\delta^{13}C$ values, two of the lower elevation Chilean Andes samples (Elq13-3550-20 and Elq13-3750-50) yield $\delta^{13}C$ values that fall within the range of expected carbonate $\delta^{13}C$ of soil carbonate forming in equilibrium with atmospheric CO_2 gas; however, the samples from the 4200 and 4500 masl sites yield $\delta^{13}C$ values higher than the expected range of equilibrium carbonate $\delta^{13}C$ values and only slightly lower than the $\delta^{13}C$ values of soil carbonates collected from the coarse-grained soils at 4700 masl. There are several possible explanations for these high $\delta^{13}C$ values, including: (1) the soil carbonates at the 4200 and 4500 masl sites formed under equilibrium conditions, and the high $\delta^{13}C$ values are due to very low soil respiration rates (Quade et al., 2007); (2) the soils carbonates from these sites formed under equilibrium conditions but experienced multiple cycles of carbonate dissolution and precipitation resulting in higher $\delta^{13}C$ values (Nakai et al., 1975; Clark and Lauriol, 1992) or (3) the soil carbonates at these sites formed via cryogenic processes leading to very positive $\delta^{13}C$ values. While the available data does not allow us to conclusively determine whether the high $\delta^{13}C$ values from these samples are the result of low soil respiration rates, dissolution-precipitation cycles, or some combination of these processes, we do reject the latter explanation (e.g., KIEs associated with bicarbonate dehydration) because in addition to causing higher than expected $\delta^{18}O$ and $\delta^{13}C$ values, cryogenic carbonate formation should also cause negative Δ_{47} anomalies. Instead we observe Δ_{47} anomalies that are indistinguishable from 0‰ and consistent with equilibrium formation, and $\delta^{18}O$ anomalies that can be explained by evaporative enrichment. Due to these observations, we suggest that the 4200 and 4500 masl samples formed under conditions of isotopic equilibrium, and that the high $\delta^{13}C$ values are the result of some other process unique to these soil sites.

Like the Tibet samples, we interpret the High Arctic sample Δ_{47} and $\delta^{18}O$ anomalies to be consistent with equilibrium carbonate formation during the summer season (Figs. 4, 5, and 7). These High Arctic samples have T(Δ_{47}) and $\delta^{18}O$ values that are consistent with local summer conditions, and Δ_{47} and $\delta^{18}O$ anomalies that—considering uncertainties in the local soil temperature and meteoric water $\delta^{18}O$ values—do not appear to be significantly different from our equilibrium soil carbonate Δ_{47} and $\delta^{18}O$ estimates. The sample from the Cannes site has Δ_{47} anomalies within error of zero; however, higher-than-expected clumped isotope temperatures (negative Δ_{47} anomalies) are observed for the Kapp Guissez samples. We suggest that these differences are likely due to two factors. First, the depth in the soil profile of the Kapp Guissez samples is unknown. The WMMT used to calculate the Kapp Guissez Δ_{47} anomalies (5 °C) is an estimate for 50

cm soil depth, but the Kapp Guissez samples may have come from shallower depths that would have experienced higher summer temperatures. Using a simple heat diffusion equation (e.g., Quade et al., 2013), we estimate that summer soil temperatures at 10 cm depth can be up to 11 °C warmer than 50 cm soil temperatures during the warmest part of the day. Second, the Kapp Guissez sample site is located ~10 km to the north of the Ny-Ålesund weather station that provides our soil and air temperature data, on a small peninsula with a south-facing aspect, exposing the soils there to more direct solar radiation than at the weather station site, which is characterized by a north-facing aspect. This difference in aspect likely results in higher surface and soil temperature at the Kapp Guissez site (Lambert and Roberts, 1976; Kang et al., 2000; Monteith and Unsworth, 2013). Taken together, we suggest that uncertainties in the exact soil depth of the Kapp Guissez samples, and variability in local climate conditions between the Kapp Guissez soil sites and the Ny-Ålesund weather station are sufficient to account for the differences between the measured Ny-Ålesund soil temperatures and the Kapp Guissez soil carbonate T(Δ_{47}) values. The $\delta^{18}O$ anomalies fall within the uncertainty of the 0‰ line regardless of whether the anomalies are calculated using the maximum or minimum meteoric water $\delta^{18}O$ estimates (Fig. 5). Based on these observations, we interpret the High Arctic as being consistent with equilibrium summer season carbonate formation.

While we do not see evidence of the High Arctic T(Δ_{47}) and $\delta^{18}O$ being significantly and systematically different from the expected equilibrium carbonate values, $\delta^{13}C$ values are very enriched relative to the $\delta^{13}C$ of local soil CO_2 (Fig. 6; Marlin et al., 1993). Unlike the Δ_{47} and $\delta^{18}O$ values, the carbonate $\delta^{13}C$ values for the Svalbard samples are inconsistent with simple equilibrium carbonate formation. The samples from both the Kapp Guissez and Cannes sites are enriched by ~4 and ~10‰ respectively, relative to the −20‰ soil CO_2 $\delta^{13}C$ values reported at the Cannes site by Marlin et al. (1993) (Fig. 6). Courty et al. (1994) reported similarly high carbonate $\delta^{13}C$ values for their soil carbonate samples, and explained them by invoking the same KIE (bicarbonate dehydration during cryogenic CO_2 degassing) that we suggested for our Antarctic and 4700 m Chilean samples. However, if we use this cryogenic carbonate formation to explain these anomalous carbonate $\delta^{13}C$ values, we would expect the carbonates to also have a positive $\delta^{18}O$ anomaly. In fact we observe the opposite, with the High Arctic Svalbard samples having negative $\delta^{18}O$ anomalies regardless of the assumed carbonate formation temperature (Fig. 5). As shown by both Clark and Lauriol (1992) and Guo (2009), the KIE associated with bicarbonate dehydration should lead to enrichment in both carbonate ^{13}C and ^{18}O, which is inconsistent with the Courty et al. (1994) interpretation. Additionally, we cannot invoke low soil respiration rates to explain the high $\delta^{13}C$ values, as we did for the 4200 and 4500 masl Chilean Andes samples, because mean annual precipitation at the High Arctic sample sites is an order of magnitude higher than at the Chilean Andes study area, which should lead to higher soil respiration rates.

Instead of invoking disequilibrium processes or low soil respiration rates, we propose that the High Arctic Svalbard soil carbonates precipitated under conditions of isotopic equilibrium, but that the carbonate $\delta^{13}C$ values for samples from both sites have been enriched in ^{13}C due to repeated cycles of dissolution and reprecipitation. Nakai et al. (1975) and Clark and Lauriol (1992) both proposed dissolution-precipitation cycles as a method for enriching carbonate ^{13}C. Using the model and equations described in Nakai et al. (1975) (see also Clark and Lauriol, 1992) we assume that an initial equilibrium carbonate precipitated in a Svalbard soil would have a carbonate $\delta^{13}C$ value of $-4‰$ based on measured soil CO_2 $\delta^{13}C$ value of $-20‰$ at the Cannes site and the $CaCO_3$-CO_2 fractionation factor of $16‰$ of Bottinga (1968). The model assumes that the initial soil carbonate undergoes partial dissolution, producing 2 mol of HCO_3^- with a $\delta^{13}C$ value of $-6.4‰$. Subsequent precipitation of calcite produces 1 mol of CO_2 gas with a $\delta^{13}C$ value of $-17.3‰$, and 1 mol of $CaCO_3$ with a $\delta^{13}C$ value of $-1.3‰$. Repeated cycles of similar dissolution and reprecipitation would result in a final soil carbonate $\delta^{13}C$ value of $+1.4‰$. This is in good agreement with the $\sim 0‰$ $\delta^{13}C$ observed at the Kapp Guissez site, and slightly less than the $5‰$ $\delta^{13}C$ at the Cannes site. Courty et al. (1994) describes the environment of the Cannes soil site as a polar desert, suggesting that lower soil respiration rates may explain the slightly higher $\delta^{13}C$ value of the Cannes-62 sample. Additional support for $\delta^{13}C$ enrichment through dissolution and reprecipitation comes from the common dissolution features noted by Courty et al. (1994) on the carbonate pendants, suggesting that carbonate dissolution and reprecipitation is an active process in the Svalbard soils.

5.1.2. Disequilibrium effects in coarse-matrix cryogenic soil carbonates from Antarctica and the Chilean Andes

The coarse-matrix soil carbonates from Antarctica and the 4700 masl Chilean Andes site can be positively identified as *cryogenic* soil carbonates based on their isotopic anomalies. Regardless of the assumed temperature of carbonate formation, the estimated disequilibrium in the Antarctic and 4700 masl Chilean soil carbonates results in negative Δ_{47} anomalies and positive $\delta^{18}O$ anomalies, though one of the 4700 masl Chilean samples (Elq13-4700-20) plots very close to the Δ_{47} origin (Fig. 7). Similarly, at all estimated formation temperatures, the $\delta^{13}C$ values of these carbonates are higher than the expected $\delta^{13}C$ of carbonates formed in equilibrium with atmospheric CO_2, which should be the upper boundary for equilibrium soil carbonates. While arid climate processes such as evaporation and low soil respiration may be responsible for some of the observed enrichment in ^{18}O and ^{13}C (Liu et al., 1996; Quade et al., 2007), these processes are insufficient to completely explain the very positive soil carbonate $\delta^{18}O$ and $\delta^{13}C$. For example, in the Atacama Desert—which is more arid than our Chilean study area—Quade et al. (2007) observed soil carbonate $\delta^{18}O$ anomalies of up to 10‰, and soil carbonate $\delta^{13}C$ values up to 7.3‰. In contrast, in our Antarctic and 4700 masl Chilean Andes samples, we observe $\delta^{18}O$ anomalies as high as 14‰, and soil carbonate $\delta^{13}C$ values up to 10.4‰. Only kinetic fractionation processes associated with rapid bicarbonate dehydration during solution freezing can explain the large magnitude of the highly positive $\delta^{13}C$ *and* $\delta^{18}O$, and the negative Δ_{47} anomalies observed in our coarse-grained matrix samples (Burgener et al., 2016).

We suggest that cryogenic carbonate formation occurs in the Antarctic and 4700 masl Chilean soils, but not at our other sample sites (3550, 3750, 4200, and 4500 masl Chilean Andes, Argentinian Andes, High Arctic, and Tibetan Plateau) due to differences in inter-cobble matrix grain size. While all of the soils described in this study have large cobbles, the Antarctic and 4700 masl Chilean soils are characterized by inter-cobble matrices that are coarse-grained (gravel-, pebble-, and sand-sized grains). In contrast, the inter-cobble matrices of the Argentinian, High Arctic and Tibetan Plateau soils all have a fine-grained component (silt sized or finer), and while the inter-cobble matrix of the lower elevation Chilean soils are dominated by sand-sized particles, they are all much more compacted than the 4700 m site. At the Arctic Svalbard site, this fine-grained component consists of dolomitic silt, while all of the Tibetan Plateau sites contain thick loess deposits that either cap the soils or form part of the inter-cobble matrix. These differences in grain size (and compaction for the four lower elevation Chilean sites) likely have a profound impact on variations in soil moisture fluctuations throughout the year, which in turn impacts the timing and style of carbonate precipitation.

It has been shown that soil sediment size plays a key role in facilitating or inhibiting CO_2 efflux out of a surface. Bouma and Bryla (2000) conducted experiments varying soil moisture and sediment size in three soil columns. They found that when irrigated, the CO_2 efflux from fine-textured soils declined drastically, and soil CO_2 concentration increased. In contrast, coarse-grained, sandy soils showed a smaller decrease in CO_2 efflux, a faster return to pre-irrigation CO_2 efflux levels, and total lower soil CO_2 concentrations following irrigation (Bouma and Bryla, 2000). The authors attributed these differing soil CO_2 responses to two factors: (1) coarse-grained soils have a larger pore-space volume than fine-grained soils (the study reported that total porosity decreased from 51% for an experimental soil composed of 96% sand, to 40% for an experimental soil composed of 45% silt and 28% clay), and (2) coarse-grained soils tend to dry faster than fine-grained soils after a wetting episode. Because of their larger pore space, coarse-grained soils preserve more open, interconnected passages for CO_2 transport and efflux even when the soil is wet, while the smaller poor spaces of finer-grained soils tend to be clogged by soil water during wetting episodes, inhibiting CO_2 transport and efflux. This observation is consistent with a compilation of permeability values for a suite of soils with grain sizes ranging from gravel to clay, which shows that soil permeability ranges from a high of 5.0×10^{-2} m s^{-1} for graded gravels with little to no fines, to as low as 7.0×10^{-10} m s^{-1} for compacted silts (Leonards, 1962; Carter and Bentley, 1991; Swiss Standard SN 670 010b, 1999; West, 2010; Dysli and Steiner, 2011). Based on these findings, we suggest that the rate of bicarbonate dehydration—and

associated CO_2 degassing in cryogenic soils—is limited by the soil pore space and permeability. Soils with coarse-grained inter-cobble matrices permit rapid CO_2 degassing, leading to the KIE observed in our Antarctic and Chilean carbonate samples. Soils with finer grained inter-cobble matrices, such as the Tibet, 3550 masl Chilean, and Svalbard High Arctic sites, inhibit CO_2 degassing by reducing CO_2 efflux from the soil and increasing CO_2 concentration within the soils. Carbonate formation at the latter soils would thus be restricted to "normal" equilibrium growth during the summer season.

We note that other processes related to, or independent of, soil sediment grain size, may also play a role in determining whether a particular cold-climate soil produces cryogenic soil carbonates. For example, under equal climate conditions, fine-grained soils will be wetter than coarse-grained soils, due to their lower porosity and permeability. During freezing events, the temperature of wetter soils will take longer to drop below 0 °C due to the "zero curtain effect", which refers to the effect of latent heat in sustaining soil temperatures near 0 °C during freezing or thawing events (Romanovsky and Osterkamp, 2000; Outcalt et al., 1990). Importantly, the duration of this zero curtain effect is controlled in part by the amount of moisture in the soil (e.g., wetter soils experience a longer zero curtain effect; Kelley and Weaver, 1969). In some locations, the zero-curtain effect has been observed to keep soil temperatures near 0 °C for up to a month (Kelley and Weaver, 1969). It is possible that a delay in complete freezing of any soil water due to the zero curtain effect could provide sufficient time for the DIC pool in a fine-grained soil to reach clumped and stable isotopic equilibrium, meaning that any soil carbonates produced in such a soil would not record the KIEs associated with bicarbonate dehydration.

In contrast, the presence or absence of a winter snowpack over a soil is not dependent on the soil matrix grain size, but may still affect whether or not cryogenic carbonate formation occurs. The presence of an overlying snowpack increases soil CO_2 concentrations by acting as an impermeable barrier that traps gases within the soil (Hinkle, 1994). Solomon and Cerling (1987) developed a model that showed the soil CO_2 concentrations at 35 cm depth increased by 15 times due to the presence of a snowpack. Higher soil CO_2 concentrations would limit CO_2 degassing from the soil water DIC pool and may even drive Eq. (3) to the left, resulting in calcite dissolution. Under such circumstances cryogenic carbonate formation would be unlikely to occur.

However, we note that potential snowpack effects are unlikely to be a factor in most of our study areas due to the local arid at those sites. Accurate, long-term measurements of snowfall at the Antarctic and 4700 masl Chilean site are unavailable (Hagedorn et al., 2007), but a review of Landsat imagery suggests that extended periods of snow cover at all of the Chilean soil sites are rare (LAND-SAT 1–5 MSS, 4–5 TM, and 7 ETM images from the USGS Earth Explorer web page, www.earthexplorer.usgs.gov). In the

Dry Valleys, Antarctica, snowfall is also rare and can be as low as 7 mm per year (Hagedorn et al., 2007), though some studies suggest long-term snowfall rates are 100–200 mm annually (Schwertferger, 1984). Additionally, weather station data from the three Tibetan Plateau sites (Lhasa, Shigatse, and T'u-ko-erh-ho-kung) record almost no snowfall over the period 1980 to 2000, which is consistent with the dry winter, wet summer climate systems that dominate the Tibetan Plateau. Landsat imagery from the three Tibetan Plateau sites largely agrees with the weather station data; while imagery from the T'u-ko-erh-ho-kung region suggests that brief snowfall events are more common in that area, the snow typically melts within a matter of days. We suggest that at such arid sites, the impact of snow cover on cryogenic carbonate development is negligible. In contrast, over the period 2008–2015, weather station data from Ny-Ålesund shows mean winter snow depths of 27 cm (maximum: 43 cm, minimum: 10 cm, $\sigma = 16$ cm), suggesting that snow effects could play a role in inhibiting the formation of cryogenic carbonates at the two Svalbard soil sites.

5.2. Isotopic disequilibrium in sub-glacial carbonates

We expected to observe evidence of KIE in sub-glacial carbonates due to the narrowly constrained, cryogenic temperature range of carbonate formation in the sub-glacial environment (−1 to 0 °C) as described in Section 2.1. Consistent with this hypothesis, the sub-glacial carbonates from Blackfoot and Castleguard glaciers both have large negative Δ_{47} anomalies. However, the $\delta^{18}O$ anomalies are more variable in terms of both magnitude and sign. Like the Antarctic and Chilean soil carbonates, the Castleguard glacier carbonates have a negative Δ_{47} anomaly and a positive $\delta^{18}O$ anomaly; however, the mean Δ_{47} anomaly of the Castleguard glacier carbonates is an order of magnitude larger than that of the coarse-matrix soil carbonates from Antarctica and the 4700 masl Chilean Andes site (−0.27‰ versus −0.023 to −0.060‰, respectively), while the $\delta^{18}O$ anomaly is slightly smaller (4.1‰ versus 9.1 to 11.2‰). The negative Δ_{47} anomaly and positive $\delta^{18}O$ anomaly observed in the Castleguard glacier carbonates are consistent with the direction of KIE associated with rapid CO_2 degassing via bicarbonate dehydration, as hypothesized for the coarse-matrix Antarctic and 4700 masl Chilean soil carbonates; however, the fact that the Castleguard glacier carbonate Δ_{47} anomalies are more than an order of magnitude larger than the coarse-matrix Antarctic and 4700 masl Chilean Δ_{47} anomalies suggest that there is some fundamental difference between cryogenic carbonate precipitation in the sub-glacial and soil environments.

In contrast to the Castleguard glacier carbonates, the Δ_{47} and $\delta^{18}O$ anomalies calculated for the Blackfoot glacier carbonates are both negative (−0.078 and −7.52‰ respectively for Δ_{47} and $\delta^{18}O$). The Δ_{47} and $\delta^{18}O$ anomalies are broadly consistent with the KIE associated with a high pH environment (Fig. 3), but we lack pH data for the sub-glacial environment at Blackfoot glacier to confirm this

possibility. Unlike the negative Δ_{47} and $\delta^{18}O$ anomalies, our Blackfoot glacier samples yield $\delta^{13}C$ values that are slightly more negative than those reported in Hanshaw and Hallet (1978), but that appear to be in isotopic equilibrium with the local carbonate bedrock.

We speculate that the difference in magnitudes of the Δ_{47} anomalies, and the different signs of $\delta^{18}O$ anomalies for the sub-glacial carbonates from the two different sites, is likely due to differences in meltwater salinity caused by variations in sub-glacial plumbing. Hanshaw and Hallet (1978) proposed that sub-glacial meltwater flow could be divided into two different end-member states. (1) In the "local flow" model, the sub-glacial film (from which the sub-glacial carbonates precipitate) is isolated from the bulk of the sub-glacial meltwater, which is funneled to the glacial tongue via discrete channels and/or tunnels. (2) In the "through-flow" model, most of the sub-glacial meltwater is distributed throughout the sub-glacial film, and thus free to interact with the carbonate precipitating solution. We suggest that salinity levels in the "local flow" model may reach much higher levels than in the "through-flow" model, due to the isolated nature of the sub-glacial films. Hill et al. (2014), have shown that in solutions where salinity is at least $50 \, g \, kg^{-1}$, KIEs that are typically associated with pH levels > 10 will manifest at lower pH levels (pH = 8–9). Hanshaw and Hallet (1978) argued that sub-glacial flow beneath Blackrock glacier is most similar to the "local flow" model. We propose that this local flow style resulted in higher salinity levels in the sub-glacial films and a lower pH threshold for the onset of KIEs, which explains why the Blackfoot sub-glacial carbonate Δ_{47} and $\delta^{18}O$ anomalies are consistent with the positive pH effect as illustrated in Fig. 7. In contrast, the sub-glacial flow beneath Castleguard glacier may be more characteristic of the "through-flow" model, resulting in lower salinity levels that favor KIEs driven by cryogenic carbonate formation and bicarbonate dehydration (resulting in negative Δ_{47} anomalies and positive $\delta^{18}O$ anomalies) rather than KIEs associated with the pH effect. Future work should focus on testing this hypothesis by making direct measurements of glacier meltwater pH and investigating how different styles of sub-glacial water flow affect meltwater salinities and resulting carbonate records.

Despite their well constrained formation temperatures and expected equilibrium $\delta^{18}O$ values, the sub-glacial carbonates proved to have larger and more variable Δ_{47} and $\delta^{18}O$ anomalies than the soil carbonates, making it a challenge to meaningfully compare and contrast the two different carbonate types. It is clear that sub-glacial carbonates are affected by a variety of formation processes, as detailed in Fairchild et al. (1994), and that this in turn can have a dramatic impact on their isotopic compositions. The Δ_{47} compositions of sub-glacial carbonates likely will not be useful in paleoclimate reconstructions or in reconstructing the oxygen isotope composition of paleo-glaciers, but they do offer unique insight into the formation processes of sub-glacial carbonates—and may present the intriguing possibility that sub-glacial carbonate Δ_{47} and $\delta^{18}O$ anomalies can be used to identify differences in the sub-glacial plumbing of ancient glaciers.

5.3. Implications for paleoclimate and paleoaltimetry reconstructions from soil carbonates

The results of this study provide a benchmark for testing whether the findings of past studies of soil carbonates may have been affected by the inclusion of disequilibrium cryogenic soil carbonates. For example, Quade et al. (2011) reported apparent $T(\Delta_{47})$ values from nine soil carbonate samples that were higher than modeled soil temperatures (e.g., the soil carbonate Δ_{47} values were lower than expected). They suggested that the discrepancy was simply the result of inaccurate modeling of local soil temperatures. Burgener et al. (2016) presented the alternative hypothesis that a cryogenic origin might explain the low Δ_{47} values, but did not attempt to calculate Δ_{47} and $\delta^{18}O$ anomalies for the Tibetan samples. The new Δ_{47}, $\delta^{18}O$, $\delta^{13}C$ values reported in this study, along with actual measurements of local summer temperatures, show that the Tibetan samples are not cryogenic in origin and are in fact consistent with the expected equilibrium carbonate isotope composition.

Our findings have important implications for terrestrial paleoclimate and paleoelevation studies. Soils with coarse-grained inter-cobble matrices in high latitude and high elevation sites are likely to produce disequilibrium soil carbonate pendants and should be avoided for quantitative paleoclimate and paleoelevation reconstructions. However, soil carbonates from high elevation sites may still provide important information about a region's tectonic and climate history. For example, soil carbonate-based paleoelevation studies typically rely on the well-known negative correlation between soil carbonate $\delta^{18}O$ and elevation, and the positive correlation between environmental temperatures estimated using Δ_{47} and elevation (Fig. 9a). Abrupt departures from that pattern (e.g., an abrupt increase in $\delta^{18}O$ and decrease in Δ_{47} with increasing elevation) may be evidence of a rapid shift to a cryogenic environment (Fig. 9b) due to uplift or climate change. Additionally, with regard to carbonate-bearing soils in deep time, the presence or absence of soil carbonate pendants that exhibit Δ_{47} and $\delta^{18}O$ anomalies indicative of cryogenic KIEs could provide constraints on the latitudinal limits of cold environments during greenhouse periods such as the Cretaceous and Eocene.

In contrast, high latitude and high elevation soils with a fine-grained inter-cobble matrix should produce equilibrium soil carbonates that are suitable for paleoclimate reconstructions. Past studies (e.g., Vogt and Corte, 1996) have identified Pleistocene and Holocene calcic paleosols with fine-grained inter-cobble matrices in current or former cold-climate environments. Such soils may offer an important window into how different terrestrial environments (e.g., mountains high elevation sites versus low elevation, high latitude sites) responded to rising temperatures and changing precipitation patterns following deglaciation at the Pleistocene/Holocene boundary.

Importantly, our findings suggest that carbonate-bearing soils that are appropriate for paleoclimate studies can be identified in the field using observations of soil matrix grain size, which should enable fieldworkers to rapidly identify soil carbonates that are likely to yield
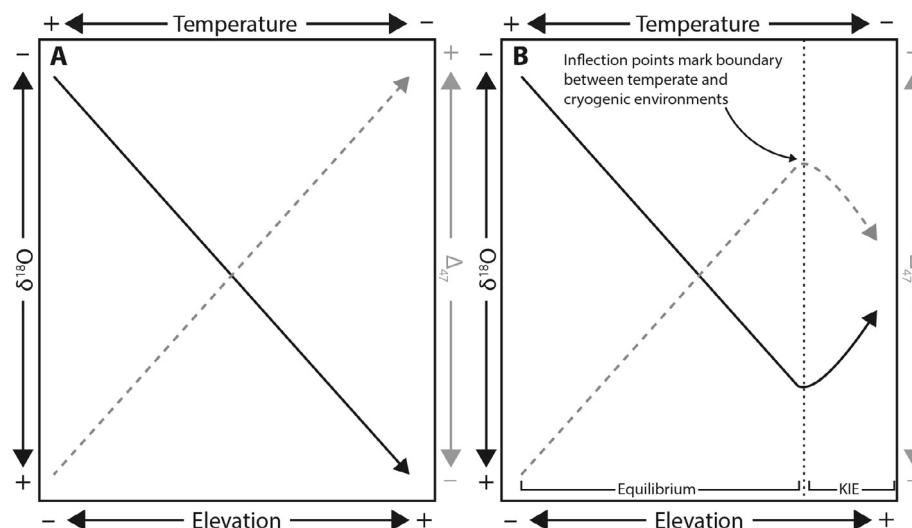
Fig. 9. Schematic illustration showing how kinetic isotope effects (KIE) associated with cryogenic carbonate formation can affect the relationship between $\delta^{18}O$, Δ_{47} and elevation. Panel A shows the typical negative correlation between soil carbonate $\delta^{18}O$ (black line) and elevation, and the typical positive correlation between soil carbonate Δ_{47} (dashed gray line) and elevation or temperature. Panel B illustrates how a transition from a typical warm or temperature climate to a cold climate at high elevation (marked by vertical dotted line) may result in high elevation soil carbonates that have increasing $\delta^{18}O$ values (positive $\delta^{18}O$ anomaly as calculated in this paper) and decreasing Δ_{47} values (negative Δ_{47} anomaly). Identification of such signals in paleoclimate datasets will help identify temporal or spatial transitions to cold climates.

equilibrium Δ_{47}, $\delta^{18}O$, $\delta^{13}C$ values. Our work also highlights the complementary nature of clumped and conventional stable isotope analyses to identify and understand disequilibrium processes in soil carbonates. For example, based on Δ_{47} or $\delta^{18}O$ values alone, it would be very difficult to determine whether our 4700 masl Chilean Andes samples represent equilibrium soil carbonates with a warm season bias, or cryogenic carbonates with lower-than-expected Δ_{47} due to KIEs; however, by using Δ_{47} and $\delta^{18}O$ anomalies in tandem, with supporting information from a comparison of expected and observed carbonate $\delta^{13}C$ values, we can positively identify the carbonates as having been affected by disequilibrium processes. Finally, our findings also point to the need for additional work to improve our understanding of how soil moisture and soil grain size interact to affect soil carbonate formation, both in terms of the timing of carbonate formation, and in terms of equilibrium versus disequilibrium isotope processes.

We note that other kinetic processes have been implicated as sources of disequilibrium isotope compositions in pedogenic carbonates from the Mojave Desert and Hawaii. McFadden et al. (1998) described carbonate "collars" that occur on large surficial clasts of Holocene and Pleistocene soils in the Mojave Desert and yield enriched $\delta^{18}O$ and $\delta^{13}C$ values relative to the isotopic composition of local waters and soil CO_2. They attributed these heavy carbonate $\delta^{18}O$ and $\delta^{13}C$ values to rapid soil water evaporation that preferentially removed ^{18}O and ^{13}C from the soil solution. Quade et al. (2013) reported very low Δ_{47} values (high T(Δ_{47}) temperatures) for fissure-filling soil carbonates in Hawaii. They hypothesized that because these carbonates were exposed to advecting air, they might have been

affected by kinetic isotope effects. Together with our own study of cryogenic soil carbonates, these studies show that soil carbonates may be affected by any number of different kinetic, non-equilibrium processes depending on climatic and soil conditions. The same approach of paired clumped and stable isotope investigations employed in this study to identify and constrain cryogenic kinetic isotope effects can be used to better characterize the disequilibrium processes associated with the Mojave soil carbonate collars and the Hawaii fissure carbonates.

We suggest that future studies of kinetic isotope effects in cryogenic soil carbonates should focus on three key areas: First, do cryogenic soil carbonates have distinct crystal growth structures, grain sizes, and crystal forms that are distinct from the calcite morphology of equilibrium soil carbonates? Second, why do cryogenic soil (this study) and cave carbonates (Kluge et al., 2014) fall off the 0.02‰ Δ_{47}-$\delta^{18}O$ correlation line modeled by Guo (2009) for bicarbonate dehydration? Third, future studies should target soils and environments that will allow a rigorous study of how other processes beyond soil sediment grain size (e.g., soil moisture, presence/absence of snow cover) inhibit or promote cryogenic soil carbonate formation.

6. CONCLUSIONS

Our findings show that soil matrix grain size plays a critical role in determining whether soil carbonates from cold climates precipitate under conditions of isotopic equilibrium or disequilibrium (Fig. 7). Arid soils with coarse-grained inter-cobble matrices are more susceptible to KIEs associated with bicarbonate dehydration, due to rapid CO_2

degassing. In contrast, soils with high soil moisture levels and fine-grained inter-cobble matrices experience reduced rates of soil CO_2 degassing, which inhibits the KIEs associated with bicarbonate dehydration during carbonate precipitation. Our findings provide important new information about (1) the importance of both annual changes to soil moisture and soil sediment size in controlling the timing and style of soil carbonate formation (e.g., Burgener et al., 2016; Gallagher and Sheldon, 2016); (2) the utility of paired clumped and stable isotope studies in identifying and describing disequilibrium processes in carbonate formation; and (3) guidelines for determining whether past studies of soil carbonates may have been influenced by the presence of disequilibrium carbonates.

The Δ_{47}, $\delta^{18}O$, $\delta^{13}C$, and calculated Δ_{47} and $\delta^{18}O$ anomalies of the Blackfoot and Castleguard glaciers are highly variable, and we attribute this observed variability to differences in sub-glacial water flow, as discussed by Hanshaw and Hallet (1978). In glaciers that experience "local flow" (e.g., channelized sub-glacier meltwater flow), the isolated pockets of meltwater film may see increased salinity levels that result in a prominent pH effect that is manifested as negative Δ_{47} and $\delta^{18}O$ anomalies. Alternatively, in glaciers characterized by a "through-flow" regime (e.g., distributed meltwater flow across the entire base of a glacier) salinity levels likely remain low and bicarbonate dehydration associated with cryogenic carbonate formation is the dominant KIE process. Currently, no pH data exists for waters derived from the two glaciers analyzed in this study. In order to better characterize the clumped isotope composition of sub-glacial carbonates, and understand their formation processes, future modeling and sampling work should focus on constraining sub-glacial solution pH and solute chemistry at the many sites where sub-glacial carbonates have been identified.

Our results suggest that high latitude and high elevation soil carbonates from soils with a fine grained inter-cobble matrix are a useful archive of paleoclimate conditions in environments that are particularly vulnerable to climate change. Such soil carbonates should be targeted in future studies to better understand how high latitude and high elevation regions responded to previous periods of climate change, such as the repeated transitions from glacial to interglacial climates that have occurred over the course of the Pleistocene and Holocene.

APPENDIX A. SUPPLEMENTARY MATERIAL

Supplementary data associated with this article can be found, in the online version, at https://doi.org/10.1016/j.gca.2018.06.006.

REFERENCES

Affek H. P., Matthews A., Ayalon A., Bar-Matthews M., Burstyn Y., Zaarur S. and Zilberman T. (2014) Accounting for kinetic isotope effects in Soreq Cave (Israel) speleothems. *Geochim. Cosmochim. Acta* **143**, 303–318. https://doi.org/10.1016/j.gca.2014.08.008.

Affek H. P. and Zaarur S. (2014) Kinetic isotope effect in CO_2 degassing: Insight from clumped and oxygen isotopes in laboratory precipitation experiments. *Geochim. Cosmochim. Acta* **143**, 319–330. https://doi.org/10.1016/j.gca.2014.08.005.

Beck W. C., Grossman E. L. and Morse J. W. (2005) Experimental studies of oxygen isotope fractionation in the carbonic acid system at 15°, 25°, and 40 °C. *Geochim. Cosmochim. Acta* **69** (14), 3493–3503. https://doi.org/10.1016/j.gca.2005.02.003.

Bottinga Y. (1968) Calculation of fractionation factors for carbon and oxygen isotopic exchange in the system calcite-carbon dioxide-water. *J. Phys. Chem.* **72**(3), 800–808. https://doi.org/10.1021/j100849a008.

Bouma T. J. and Bryla D. R. (2000) On the assessment of root and soil respiration for soils of different textures: interactions with soil moisture contents and soil CO_2 concentrations. *Plant Soil* **227**, 215–221. https://doi.org/10.1023/A:1026502414977.

Brady N. C. and Weil R. R. (2010) *Elements of the Nature and Properties of Soils*, 3rd ed. Pearson.

Brand W. A., Assonov S. S. and Coplen T. B. (2010) Correction for the ^{17}O interference in $\delta(^{13}C)$ measurements when analyzing CO_2 with stable isotope mass spectrometry (IUPAC Technical Report). *Pure Appl. Chem.* **82**(8), 1719–1733. https://doi.org/10.1351/PAC-REP-09-01-05.

Breecker D. O., Sharp Z. D. and McFadden L. D. (2009) Seasonal bias in the formation and stable isotopic composition of pedogenic carbonate in modern soils from central New Mexico, USA. *Geol. Soc. Am. Bull.* **121**(3–4), 630–640. https://doi.org/10.1130/B26413.1.

Bunting B. T. and Christensen L. (1978) Micromorphology of calcareous crusts from the Canadian High Arctic. *Geologiska Föreningen I Stockholm Förhandlingar* **4**, 361–367.

Burgener L., Huntington K. W., Hoke G. D., Schauer A., Ringham M. C., Latorre C. and Díaz F. P. (2016) Variations in soil carbonate formation and seasonal bias over >4 km of relief in the western Andes (30°S) revealed by clumped isotope thermometry. *Earth Planet. Sci. Lett.* **441**, 188–199. https://doi.org/10.1016/j.epsl.2016.02.033.

Campbell B., Claridge G. G. C., Zealand N., Campbell D. I., and Balks M. R. (1998) Soil environment of the Mcmurdo dry valleys, Antarctica The soils in the McMurdo Dry Valley region are a key component in an environment of low precipitation, severe cold and minimal biological activity, the soils have distinctive of oxidation for vari.

Carrapa B., Huntington K. W., Clementz M., Quade J., Bywater-Reyes S., Schoenbohm L. M. and Canavan R. R. (2014) Uplift of the central andes of NW Argentina associated with upper crustal shortening, revealed by multiproxy isotopic analyses. *Tectonics* **33**(6), 1039–1054. https://doi.org/10.1002/2013TC003461.

Carter M. and Bentley S. (1991) *Correlations of Soil Properties*. Pentech Press Publishers, Lond.

Cerling T. and Quade J. (1993) Stable carbon and oxygen isotopes in soil carbonates. Geophysical Monograph Series. pp. 217–231. Retrieved from http://www.agu.org/books/gm/v078/GM078p0217/GM078p0217.shtml.

Clark I. D. and Lauriol B. (1992) Kinetic enrichment of stable isotopes in cryogenic calcites. *Chem. Geol.* **102**(1–4), 217–228. https://doi.org/10.1016/0009-2541(92)90157-Z.

Courty M. A., Marlin C., Dever L., Tremblay P. and Vachier P. (1994) The properties, genesis and environmental significance of calcitic pendents from the High Arctic (Spitsbergen). *Geoderma* **61**(1–2), 71–102. https://doi.org/10.1016/0016-7061(94)90012-4.

Daëron M., Blamart D., Peral M. and Affek H. P. (2016) Absolute isotopic abundance ratios and the accuracy of Δ_{47} measurements. *Chem. Geol.* **442**, 83–96. https://doi.org/10.1016/j.chemgeo.2016.08.014.

Daëron M., Guo W., Eiler J., Genty D., Blamart D., Boch R., Drysdale R., Maire R., Wainer K. and Zanchetta G. (2011) $^{13}C^{18}O$ clumping in speleothems: Observations from natural caves and precipitation experiments. *Geochim. Cosmochim. Acta* **75**(12), 3303–3317. https://doi.org/10.1016/j.gca.2010.10.032.

Defliese W. F. and Lohmann K. C. (2015) Non-linear mixing effects on mass-47 CO_2 clumped isotope thermometry: patterns and implications. *Rapid Commun. Mass Spectrom.* **29**(9), 901–909. https://doi.org/10.1002/rcm.7175.

Dennis K. J., Affek H. P., Passey B. H., Schrag D. P. and Eiler J. M. (2011) Defining an absolute reference frame for "clumped" isotope studies of CO_2. *Geochim. Cosmochim. Acta* **75**(22), 7117–7131. https://doi.org/10.1016/j.gca.2011.09.025.

Dennis K. J. and Schrag D. P. (2010) Clumped isotope thermometry of carbonatites as an indicator of diagenetic alteration. *Geochim. Cosmochim. Acta* **74**(14), 4110–4122. https://doi.org/10.1016/j.gca.2010.04.005.

DePaolo D. J. (2011) Surface kinetic model for isotopic and trace element fractionation during precipitation of calcite from aqueous solutions. *Geochim. Cosmochim. Acta* **75**(4), 1039–1056. https://doi.org/10.1016/j.gca.2010.11.020.

Devriendt L. S., Watkins J. M. and McGregor H. V. (2017) Oxygen isotope fractionation in the $CaCO_3$-DIC-H_2O system. *Geochim. Cosmochim. Acta* **214**, 115–142. https://doi.org/10.1016/j.gca.2017.06.022.

Diaz N., King G. E., Valla P. G., Herman F. and Verrecchia E. P. (2016) Pedogenic carbonate nodules as soil time archives: challenges and investigations related to OSL dating. *Quat. Geochronol.* **36**, 120–133. https://doi.org/10.1016/j.quageo.2016.08.008.

Dietrich F., Diaz N., Deschamps P., Ngounou Ngatcha B., Sebag D. and Verrecchia E. P. (2017) Origin of calcium in pedogenic carbonate nodules from silicate watersheds in the Far North Region of Cameroon: respective contribution of in situ weathering source and dust input. *Chem. Geol.* **460**, 54–69. https://doi.org/10.1016/j.chemgeo.2017.04.015.

Dietzel M., Tang J., Leis A. and Köhler S. J. (2009) Oxygen isotopic fractionation during inorganic calcite precipitation - effects of temperature, precipitation rate and pH. *Chem. Geol.* **268**(1–2), 107–115. https://doi.org/10.1016/j.chemgeo.2009.07.015.

Dysli M. and Steiner W. (2011) *Correlations in Soil Mechanics*. PPUR Polytechnic Press, Italy.

Eagle R. a., Risi C., Mitchell J. L., Eiler J. M., Seibt U., Neelin J. D., Gaojun L. and Tripati A. K. (2013) High regional climate sensitivity over continental China constrained by glacial-recent changes in temperature and the hydrological cycle. *PNAS* **110**(22), 8813–8818. https://doi.org/10.1073/pnas.1213366110.

Eiler J. M. and Schauble E. (2004) $^{18}O^{13}C^{16}O$ in Earth's atmosphere. *Geochim. Cosmochim. Acta* **68**(23), 4767–4777. https://doi.org/10.1016/j.gca.2004.05.035.

Fairchild I. J., Bradby L., Spiro B. and Project I. G. C. (1994) Reactive carbonate in glacial systems: a preliminary synthesis of creation, dissolution and reincarnation. *Earth's Glacial Rec.* **260**, 176–192.

Fairchild I. J., Frisia S., Borsato A. and Tooth A. F. (2007) Speleothems. In *Geochemical Sediments and Landscapes* (eds. D. J. Nash and S. J. McLaren). Blackwell Publishing, Malden, MA.

Foley K. K. (2005) *Pedogenic carbonate distribution within glacial till in Taylor Valley, Southern Victoria Land*. The Ohio State University, Antarctica.

Forman S. L. and Miller G. H. (1984) Time-dependent soil morphologies and pedogenic processes on raised beaches, Bröggerhalvöya, Spitsbergen, Svalbard Archipelago. *Arct. Alp. Res.* **16**, 381–394. https://doi.org/10.2307/1550900.

Gabitov R. I., Watson E. B. and Sadekov A. (2012) Oxygen isotope fractionation between calcite and fluid as a function of growth rate and temperature: an in situ study. *Chem. Geol.* **306–307**, 92–102. https://doi.org/10.1016/j.chemgeo.2012.02.021.

Gallagher T. M. and Sheldon N. D. (2016) Combining soil water balance and clumped isotopes to understand the nature and timing of pedogenic carbonate formation. *Chem. Geol.* **435**, 79–91. https://doi.org/10.1016/j.chemgeo.2016.04.023.

Garzione C. N., Auerbach D. J., Jin-Sook Smith J., Rosario J. J., Passey B. H., Jordan T. E. and Eiler J. M. (2014) Clumped isotope evidence for diachronous surface cooling of the Altiplano and pulsed surface uplift of the Central Andes. *Earth Planet. Sci. Lett.* **393**, 173–181. https://doi.org/10.1016/j.epsl.2014.02.029.

Ghosh P., Garzione Carmala N. and Eiler J. M. (2006) Rapid uplift of the Altiplano revealed through ^{13}C-^{18}O bonds in paleosol carbonates. *Science* **311**(January), 511–515.

Gile L., Peterson F. and Grossman R. (1966) Morphological and genetic sequences of carbonate accumulation in desert soils. *Soil Sci.* **101**(5), 347–360.

Gunal H. and Ransom M. D. (2006) Clay illuviation and calcium carbonate accumulation along a precipitation gradient in Kansas. *Catena* **68**(1), 59–69. https://doi.org/10.1016/j.catena.2006.04.027.

Guo W. (2009) *Carbonate Clumped Isotope Thermometry: Application to Carbonaceous Chondrites and Effects of Kinetic Isotope Fractionation*. California Institute of Technology.

Hagedorn B., Sletten R. S. and Hallet B. (2007) Sublimation and ice condensation in hyperarid soils: Modeling results using field data from Victoria Valley, Antarctica. *J. Geophys. Res. Earth Surf.* **112**(3). https://doi.org/10.1029/2006JF000580.

Hagedorn B., Sletten R. S., Hallet B., McTigue D. F. and Steig E. J. (2010) Ground ice recharge via brine transport in frozen soils of Victoria Valley, Antarctica: Insights from modeling $\delta^{18}O$ and δD profiles. *Geochim. Cosmochim. Acta* **74**(2), 435–448. https://doi.org/10.1016/j.gca.2009.10.021.

Hallet B. (1976) Deposits formed by subglacial precipitation of $CaCO_3$. *Geol. Soc. Am. Bull.* **87**(7), 1003–1015.

Hanshaw B. B. and Hallet B. (1978) Oxygen isotope composition of subglacially precipitated calcite: possible paleoclimatic implications. *Science* **200**(4347), 1267–1270 http://science.sciencemag.org/content/200/4347/1267.abstract.

He B., Olack G. A. and Colman A. S. (2012) Pressure baseline correction and high-precision CO_2 clumped-isotope (δ_{47}) measurements in bellows and micro-volume modes. *Rapid Commun. Mass Spectrom.* **26**(24), 2837–2853. https://doi.org/10.1002/rcm.6436.

Henkes G. A., Passey B. H., Wanamaker A. D., Grossman E. L., Ambrose W. G. and Carroll M. L. (2013) Carbonate clumped isotope compositions of modern marine mollusk and brachiopod shells. *Geochim. Cosmochim. Acta* **106**, 307–325. https://doi.org/10.1016/j.gca.2012.12.020.

Hill P. S., Tripati A. K. and Schauble E. A. (2014) Theoretical constraints on the effects of pH, salinity, and temperature on clumped isotope signatures of dissolved inorganic carbon species and precipitating carbonate minerals. *Geochim. Cos-*

mochim. Acta **125**, 610–652. https://doi.org/10.1016/j. gca.2013.06.018.

Hinkle M. E. (1994) Environmental conditions affecting concentrations of He, CO2, O2 and N2 in soil gases. *Appl. Geochem.* **9**(1), 53–63. https://doi.org/10.1016/0883-2927(94)90052-3.

Hitchon B. and Krouse H. (1972) Hydrogeochemistry of the surface waters of the Mackenzie River drainage basin, Canada–III. Stable isotopes of oxygen, carbon and sulphur. *Geochim. Cosmochim. Ac.* **36**, 1337–1357.

Hoke G. D., Garzione C. N., Araneo D. C., Latorre C., Strecker M. R. and Williams K. J. (2009) The stable isotope altimeter: Do Quaternary pedogenic carbonates predict modern elevations?. *Geology* **37**(11) 1015–1018. https://doi.org/10.1130/G30308A.1.

Hough B. G., Fan M. and Passey B. H. (2014) Calibration of the clumped isotope geothermometer in soil carbonate in Wyoming and Nebraska, USA: Implications for paleoelevation and paleoclimate reconstruction. *Earth Planet. Sci. Lett.* **391**, 110–120. https://doi.org/10.1016/j.epsl.2014.01.008.

Huntington K. W., Eiler J. M., Affek H. P., Guo W., Bonifacie M., Yeung L. Y., Thiagarajan N., Passey B., Tripati A., Daëron M. and Came R. (2009) Methods and limitations of "clumped" CO_2 isotope (Δ_{47}) analysis by gas-source isotope ratio mass spectrometry. *J. Mass Spectrom.* **44**(9), 1318–1329. https://doi.org/10.1002/jms.1614.

Kabala C. and Zapart J. (2012) Initial soil development and carbon accumulation on moraines of the rapidly retreating Werenskiold Glacier, SW Spitsbergen, Svalbard archipelago. *Geoderma* **175–176**, 9–20. https://doi.org/10.1016/j.geoderma.2012.01.025.

Kang S., Kim S., Oh S. and Lee D. (2000) Predicting spatial and temporal patterns of soil temperature based on topography, surface cover and air temperature. *For. Ecol. Manage.* **136**(1–3), 173–184. https://doi.org/10.1016/S0378-1127(99)00290-X.

Kelley J. J. and Weaver D. F. (1969) Physical processes at the surface of the arctic tundra. *Arctic* **22**(4), 425–437. https://doi.org/10.2307/40507880.

Kelson J. R., Huntington K. W., Schauer A. J., Saenger C. and Lechler A. R. (2017) Toward a universal carbonate clumped isotope calibration: Diverse synthesis and preparatory methods suggest a single temperature relationship. *Geochim. Cosmochim. Acta* **197**, 104–131. https://doi.org/10.1016/j.gca.2016.10.010.

Kim S. T., O'Neil J. R., Hillaire-Marcel C. and Mucci A. (2007) Oxygen isotope fractionation between synthetic aragonite and water: Influence of temperature and Mg^{2+} concentration. *Geochim. Cosmochim. Acta* **71**(19), 4704–4715. https://doi.org/10.1016/j.gca.2007.04.019.

Kim S.-T. and O'Neil J. R. (1997) Equilibrium and nonequilibrium oxygen isotope effects in synthetic carbonates. *Geochim. Cosmochim. Acta* **61**(16), 3461–3475. https://doi.org/10.1016/S0016-7037(97)00169-5.

Kluge T. and Affek H. P. (2012) Quantifying kinetic fractionation in Bunker Cave speleothems using Δ_{47}. *Quat. Sci. Rev.* **49**, 82–94. https://doi.org/10.1016/j.quascirev.2012.06.013.

Kluge T., Affek H. P., Zhang Y. G., Dublyansky Y., Spötl C., Immenhauser A. and Richter D. K. (2014) Clumped isotope thermometry of cryogenic cave carbonates. *Geochim. Cosmochim. Acta* **126**, 541–554. https://doi.org/10.1016/j.gca.2013.11.011.

Kohn M. J. (2010) Carbon isotope compositions of terrestrial C3 plants as indicators of (paleo)ecology and (paleo)climate. *PNAS* **107**(46), 19691–19695. https://doi.org/10.1073/pnas.1004933107.

Lacelle D. (2007) Environmental setting, (micro)morphologies and stable C-O isotope composition of cold climate carbonate precipitates-a review and evaluation of their potential as paleoclimatic proxies. *Quat. Sci. Rev.* **26**(11–12), 1670–1689. https://doi.org/10.1016/j.quascirev.2007.03.011.

Lachniet M. S. (2009) Climatic and environmental controls on speleothem oxygen-isotope values. *Quat. Sci. Rev.* **28**(5–6), 412–432. https://doi.org/10.1016/j.quascirev.2008.10.021.

Lambert M. G. and Roberts E. (1976) Aspect differences in an unimproved hill country pasture, 1. Climatic differences. *N. Z. J. Agric. Res.* **19**(4), 459–467. https://doi.org/10.1080/00288233.1978.10427407.

Leonards G. (1962) *Foundation Engineering*. McGraw-Hill, New York.

Licht A., Quade J., Kowler A., De Los Santos M., Hudson A., Schauer A., Huntington K., Copeland P. and Lawton T. (2017) Impact of the North American monsoon on isotope paleoaltimeters: implications for the paleoaltimetry of the American southwest. *Am. J. Sci.* **317**(1), 1–33. https://doi.org/10.2475/01.2017.01.

Liu B., Phillips F. and Campbell A. (1996) Stable carbon and oxygen isotopes of pedogenic carbonates, Ajo Mountains, southern Arizona: implications for paleoenvironmental change. *Palaeogeogr., Palaeoclimatol., Palaeoecol.* **124**, 233–246 http://www.sciencedirect.com/science/article/pii/0031018295000933.

Mann D. H., Sletten R. S. and Ugolini F. C. (1986) Soil development at Kongsfjorden, Spitsbergen. *Polar Res.* **4**(1), 1–16. https://doi.org/10.1111/j.1751-8369.1986.tb00513.x.

Marlier J. F. and O'Leary M. H. (1984) Carbon kinetic isotope effects on the hydration of carbon dioxide and the dehydration of bicarbonate ion. *J. Am. Chem. Soc.* **106**(18), 5054–5057. https://doi.org/10.1021/ja00330a003.

Marlin C., Dever L., Vachier P. and Courty M.-A. (1993) Variations chimiques et isotopique de l'eau du sol lors de la reprise en gel d'une couche active sur perigélisol continu (Presqu'ile de Brogger, Svalbard). *Can. J. Earth Sci.* **30**(Akerman 1980), 806–813. https://doi.org/10.1139/e93-066.

McCraw J. D. (1967) Soils of Taylor Dry Valley, Victoria Land, Antarctica, with notes on soils from other localities in Victoria Land. *New Zealand Journal of Geology and Geophysics* **10**(July 2014), 498–539. https://doi.org/10.1080/00288306.1967.10426754.

McFadden L. D., McDonald E. V., Wells S. G., Anderson K., Quade J. and Forman S. L. (1998) The vesicular layer and carbonate collars of desert soils and pavements: formation, age and relation to climate change. *Geomorphology* **24**(2–3), 101–145. https://doi.org/10.1016/S0169-555X(97)00095-0.

Monteith J. L. and Unsworth M. H. (2013) Principles of environmental physics. Plants, Animals and the atmosphere Illus. Paper (Vol. American), Xii+291p. Retrieved from. In *Principles of Environmental Physics* (eds. J. L. Monteith and M. H. Unsworth), second ed. Routledge, Chapman and Hall, New York, New York, USA.

Mook W. G., Bommerson J. C. and Staverman W. H. (1974) Carbon isotope fractionation between dissolved bicarbonate and gaseous carbon dioxide. *Earth Planet. Sci. Lett.* **22**(2), 169–176. https://doi.org/10.1016/0012-821X(74)90078-8.

Nakai N., Wada H., and Kiyosu Y. A. (1975) Stable isotope studies on the origin and geological history of water and salts in the Lake Yanda area, Antarctica, 9.

Outcalt S. I., Nelson F. E. and Hinkel K. M. (1990) The zero-curtain effect: Heat and mass transfer across an isothermal region in freezing soil. *Water Resour. Res.* **26**(7), 1509–1516. https://doi.org/10.1029/WR026i007p01509.

Paneth P. and O'Leary M. H. (1985) Mechanism of the Spontaneous Dehydration of Bicarbonate Ion. *J. Am. Chem. Soc.* **107**(25), 7381–7384. https://doi.org/10.1021/ja00311a027.

Passey B. H., Levin N. E., Cerling T. E., Brown F. H. and Eiler J. M. (2010) High-temperature environments of human evolution

in East Africa based on bond ordering in paleosol carbonates. *PNAS* **107**(25), 11245–11249. https://doi.org/10.1073/pnas.1001824107.

Paulik C., Melzer T., Hahn S., Bartsch A., Heim B., Elger K., and Wagner W. (2014) Circumpolar surface soil moisture and freeze/thaw surface status remote sensing products (version 4) with links to geotiff images and netCDF files (2007-01 to 2013-12).

Peters N. a., Huntington K. W. and Hoke G. D. (2013) Hot or not? Impact of seasonally variable soil carbonate formation on paleotemperature and O-isotope records from clumped isotope thermometry. *Earth Planet. Sci. Lett.* **361**, 208–218. https://doi.org/10.1016/j.epsl.2012.10.024.

Quade J., Eiler J., Daëron M. and Achyuthan H. (2013) The clumped isotope geothermometer in soil and paleosol carbonate. *Geochim. Cosmochim. Acta* **105**, 92–107. https://doi.org/10.1016/j.gca.2012.11.031.

Quade J., Breecker D. O., Daëron M. and Eiler J. (2011) The paleoaltimetry of Tibet: an isotopic perspective. *Am. J. Sci.* **311** (2), 77–115. https://doi.org/10.2475/02.2011.01.

Quade J., Rech J. a., Latorre C., Betancourt J. L., Gleeson E. and Kalin M. T. K. (2007) Soils at the hyperarid margin: the isotopic composition of soil carbonate from the Atacama Desert, Northern Chile. *Geochim. Cosmochim. Acta* **71**, 3772–3795. https://doi.org/10.1016/j.gca.2007.02.016.

Ringham M. C., Hoke G. D., Huntington K. W. and Aranibar J. N. (2016) Influence of vegetation type and site-to-site variability on soil carbonate clumped isotope records, Andean piedmont of Central Argentina (32–34° S). *Earth Planet. Sci. Lett.* **440**(June), 1–11. https://doi.org/10.1016/j.epsl.2016.02.003.

Romanovsky V. E. and Osterkamp T. E. (2000) Effects of unfrozen water on heat and mass transport processes in the active layer and permafrost. *Permafrost Periglac. Process.* **11**(3), 219–239. https://doi.org/10.1002/1099-1530(200007/09)11:3<219::AID-PPP352>3.0.CO;2-7.

Ross S. M. and Ph D. (2003) Peirce's criterion for the elimination of suspect experimental data Retrieved from. *J. Eng. Technol.* **20**, 1–12 http://classes.engineering.wustl.edu/2009/fall/che473/handouts/OutlierRejection.pdf.

Saenger C., Affek H. P., Felis T., Thiagarajan N., Lough J. M. and Holcomb M. (2012) Carbonate clumped isotope variability in shallow water corals: Temperature dependence and growth-related vital effects. *Geochim. Cosmochim. Acta* **99**, 224–242. https://doi.org/10.1016/j.gca.2012.09.035.

Schauble E. A., Ghosh P. and Eiler J. M. (2006) Preferential formation of 13C–18O bonds in carbonate minerals, estimated using first-principles lattice dynamics. *Geochim. Cosmochim. Acta* **70**(10), 2510–2529. https://doi.org/10.1016/j.gca.2006.02.011.

Schauer A. J., Kelson J., Saenger C. and Huntington K. W. (2016) Choice of ^{17}O correction affects clumped isotope (Δ_{47}) values of CO2 measured with mass spectrometry. *Rapid Commun. Mass Spectrom.* **30**(24), 2607–2616. https://doi.org/10.1002/rcm.7743.

Schwertfeger W. (1984). Weather and climate of Antarctica. New York.

Snell K. E., Thrasher B. L., Eiler J. M., Koch P. L., Sloan L. C. and Tabor N. J. (2013) Hot summers in the Bighorn Basin during the early Paleogene. *Geology* **41**(1), 55–58. https://doi.org/10.1130/G33567.1.

Solomon D. K. and Cerling T. E. (1987) The annual carbon dioxide cycle in a montane soil: observations, modeling, and implications for weathering. *Water Resour. Res.* **23**(12), 2257–2265. https://doi.org/10.1029/WR023i012p02257.

Souchez R. A. and Lemmens M. (1985) Subglacial carbonate deposition: An isotopic study of a present-day case. *Palaeo-geogr. Palaeoclimatol. Palaeoecol.* **51**(1–4), 357–364. https://doi.org/10.1016/0031-0182(85)90093-8.

Still C. J., Berry J. A., Collatz G. J. and DeFries R. S. (2003) Global distribution of C_3 and C_4 vegetation: carbon cycle implications. *Glob. Biogeochem. Cycles* **17**(1). https://doi.org/10.1029/2001GB001807, 6-1-6–14.

Swett K. (1974) Calcrete Crusts in an arctic permafrost environment. *Am. J. Sci.* **274**, 1059–1063.

Swiss Standard SN 670 010b (1999) *Characteristics Coefficients of Soils*. Association of Swiss Road and Traffic Engineers.

Tedrow J. C. F. and Ugolini F. C. (1966). Antarctic soils. Antarctic Research Series, 8.

Tripati A. K., Eagle R. A., Thiagarajan N., Gagnon A. C., Bauch H., Halloran P. R. and Eiler J. M. (2010) ^{13}C–^{18}O isotope signatures and "clumped isotope" thermometry in foraminifera and coccoliths. *Geochim. Cosmochim. Acta* **74**(20), 5697–5717. https://doi.org/10.1016/j.gca.2010.07.006.

Tripati A. K., Hill P. S., Eagle R. A., Mosenfelder J. L., Tang J., Schauble E. A., Eiler J. M., Zeebe R. E., Uchikawa J., Coplen T. B., Ries J. B. and Henry D. (2015) Beyond temperature: clumped isotope signatures in dissolved inorganic carbon species and the influence of solution chemistry on carbonate mineral composition. *Geochim. Cosmochim. Acta* **166**, 344–371. https://doi.org/10.1016/j.gca.2015.06.021.

Uchikawa J. and Zeebe R. E. (2012) The effect of carbonic anhydrase on the kinetics and equilibrium of the oxygen isotope exchange in the CO2-H2O system: implications for δ^{18}O vital effects in biogenic carbonates. *Geochim. Cosmochim. Acta* **95**, 15–34. https://doi.org/10.1016/j.gca.2012.07.022.

Usdowski E. and Hoefs J. (1993) Oxygen isotope exchange between carbonic acid, bicarbonate, carbonate, and water: a re-examination of the data of McCrea (1950) and an expression for the overall partitioning of oxygen isotopes between the carbonate species and water. *Geochim. Cosmochim. Acta* **57**(15), 3815–3818. https://doi.org/10.1016/0016-7037(93)90159-T.

Vogt T. and Corte a. E. (1996) Secondary precipitates in Pleistocene and present cryogenic environments (Mendoza Precordillera, Argentina, Transbaikalia, Siberia, and Seymour Island, Antarctica). *Sedimentology* **43**, 53–64. https://doi.org/10.1111/j.1365-3091.1996.tb01459.x.

Wacker U., Fiebig J. and Schoene B. R. (2013) Clumped isotope analysis of carbonates: comparison of two different acid digestion techniques. *Rapid Commun. Mass Spectrom.: RCM* **27**(14), 1631–1642. https://doi.org/10.1002/rcm.6609.

Wang Z., Gaetani G., Liu C. and Cohen A. (2013) Oxygen isotope fractionation between aragonite and seawater: developing a novel kinetic oxygen isotope fractionation model. *Geochim. Cosmochim. Acta* **117**, 232–251. https://doi.org/10.1016/j.gca.2013.04.025.

Watkins J. M. and Hunt J. D. (2015) A process-based model for non-equilibrium clumped isotope effects in carbonates. *Earth Planet. Sci. Lett.* **432**, 152–165. https://doi.org/10.1016/j.epsl.2015.09.042.

Watkins J. M., Nielsen L. C., Ryerson F. J. and DePaolo D. J. (2013) The influence of kinetics on the oxygen isotope composition of calcium carbonate. *Earth Planet. Sc. Lett.* **375**, 349–360. https://doi.org/10.1016/j.epsl.2013.05.054.

Watkins J. M., Hunt J. D., Ryerson F. J. and DePaolo D. J. (2014) The influence of temperature, pH, and growth rate on the δ^{18}O composition of inorganically precipitated calcite. *Earth Planet. Sci. Lett.* **404**, 332–343. https://doi.org/10.1016/j.epsl.2014.07.036.

Watson E. B. (2004) A conceptual model for near-surface kinetic controls on the trace- element and stable isotope composition of abiogenic calcite crystals. *Geochim. Cosmochim. Acta* **68**(7), 1473–1488. https://doi.org/10.1016/j.gca.2003.10.003.

Watson E. B. and Müller T. (2009) Non-equilibrium isotopic and elemental fractionation during diffusion-controlled crystal growth under static and dynamic conditions. *Chem. Geol.* **267** (3–4), 111–124. https://doi.org/10.1016/j.chemgeo.2008.10.036.

West T. (2010) *Geology Applied to Engineering*. Waveland Press, Long Grove, Illinois.

Zaarur S., Affek H. P. and Brandon M. T. (2013) A revised calibration of the clumped isotope thermometer. *Earth Planet. Sci. Lett.* **382**, 47–57. https://doi.org/10.1016/j.epsl.2013.07.026.

Zeebe R. E. (2007) An expression for the overall oxygen isotope fractionation between the sum of dissolved inorganic carbon and water. *Geochem. Geophys. Geosyst.* **8**(9), 1–7. https://doi.org/10.1029/2007GC001663.

Zeebe R. E. (1999) An explanation of the effect of seawater carbonate concentration on foraminiferal oxygen isotopes. *Geochim. Cosmochim. Acta* **63**(13–14), 2001–2007. https://doi.org/10.1016/S0016-7037(99)00091-5.

Zeebe R. E., Wolf-Gladrow D. A. and Jansen H. (1999) On the time required to establish chemical and isotopic equilibrium in the carbon dioxide system in seawater. *Mar. Chem.* **65**(3–4), 135–153. https://doi.org/10.1016/S0304-4203(98)00092-9.

Zeebe R. E. and Wolfe-Gladrow D. (2001) *CO_2 in Seawater: Equilibrium, Kinetics, Isotopes*, 1st ed. Elsevier, Amsterdam, The Netherlands.

Associate editor: Miryam Bar-Matthews